Available online at www.sciencedirect.com
SCIENCE DIRECT®
Comput. Methods Appl. Mech. Engrg. 193 (2004) 3303–3325
Computer methods in applied mechanics and engineering
www.elsevier.com/locate/cma

Application of the material force method to thermo-hyperelasticity

Ellen Kuhl, Ralf Denzer, Franz Josef Barth, Paul Steinmann *

Department of Mechanical Engineering, Chair for Applied Mechanics, University of Kaiserslautern, Postfach 3049, D-67653 Kaiserslautern, Germany

Received 14 February 2003; received in revised form 19 September 2003; accepted 21 September 2003

Abstract

The numerical analysis of material forces in the context of thermo-hyperelasticity constitutes the central topic of the present paper. In contrast to classical spatial forces in the sense of Newton, material forces in the sense of Eshelby indicate the tendency of material inhomogeneities to move relative to their surrounding material. Material forces are thus considered of particular importance in the context of thermo-elasticity where thermal effects can be understood as a potential source of inhomogeneity. The relevant balance equations of thermo-elasticity, i.e. the balance of momentum and energy, which essentially govern the evolution of the deformation and the temperature field are thus illustrated for both, the classical spatial and the material motion context. Guided by arguments of duality, the corresponding weak forms are derived. Next, we carry out the finite element discretization of both problems. While the numerical solution of the spatial motion problem renders the discrete spatial deformation map and the temperature as nodal degrees of freedom, the solution of the material motion problem provides the discrete material node point forces. The former typically relies on the solution of a global system of equations whereas the latter is introduced as a mere post-processing procedure. Since we apply a simultaneous solution of the mechanical and the thermal problem with the deformation and the temperature interpolated in a $\mathscr{C}^0$-continuous way, all the relevant information for the material force method is readily available once the spatial motion problem has been solved. Selected examples from the field of fracture mechanics illustrate the additional insight that is provided by the results of the material force method.

Keywords: Spatial and material setting; Material inhomogeneities; Material force method; Thermo-hyperelasticity

1. Introduction

Thermomechanical problems are of particular importance for a number of industrial applications in civil, mechanical or aerospace engineering. Thereby, the coupling between the mechanical and the thermal response is twofold. On the one hand, we typically encounter thermally induced stresses, i.e. the

* Corresponding author. Tel.: +49-631-205-2419; fax: +49-631-205-2128.
E-mail addresses: ekuhl@rhrk.uni-kl.de (E. Kuhl), denzer@rhrk.uni-kl.de (R. Denzer), barth@rhrk.uni-kl.de (F.J. Barth), ps@rhrk.uni-kl.de (P. Steinmann).
URL: http://mechanik.mv.uni-kl.de.

0045-7825/$ - see front matter
doi:10.1016/j.cma.2003.09.021

deformation of the structure strongly depends on the temperature field it is subjected to. On the other hand, large deformations induce structural heating, a phenomenon which is classically referred to as Gough–Joule effect. Traditionally, thermodynamic effects are characterized in the spatial motion context within the framework of rational thermodynamics, see e.g. [5,39,40] or the recent textbooks of Silhavý [32], Maugin [21], Haupt [11] or Liu [18]. Conceptually speaking, the spatial setting of continuum thermodynamics considers the response to variations of spatial placements of particles with respect to the ambient space.

In a computational context, the basic concern is the evaluation of the spatial motion balance of momentum and energy, whereby the former essentially represents the equilibrium of spatial forces in the sense of Newton. The resulting coupled system of equations defines the evolution of the spatial deformation map and the temperature field. In a finite element context, first attempts towards a numerical solution of finite thermo-elasticity date back to the early work of Oden [27]. A detailed analysis of different staggered solution techniques based on an isothermal or an adiabatic split can be found in Armero and Simo [1]. A comparison with a fully monolithic solution technique has been carried out by Miehe [22–24] and Simo [33]. In the present work, we shall focus on a simultaneous solution of the balance of momentum and energy, which has also been documented by Simo and Miehe [34], Reese and Govindjee [29], Reese and Wriggers [30], Reese [28] or Ibrahimbegovic et al. [12]. However, in contrast to the above mentioned references, we shall restrict ourselves to the thermo-hyperelastic case in the sequel.

The evolution of the deformation field and the temperature field is typically accompanied with the local rearrangement of material inhomogeneities which can be characterized elegantly within the material motion context, see e.g. the comprehensive overviews by Maugin [19,20], Gurtin [10] or Kienzler and Herrmann [13] or our own recent contributions by Steinmann [36,37] and Kuhl and Steinmann [16]. In contrast to the spatial motion setting, the material motion setting of continuum thermodynamics is concerned with the response to variations of material placements of particles with respect to the ambient material. The material motion point of view is thus extremely prominent when dealing with defect mechanics to which it has originally been introduced by Eshelby [7,8] more than half a century ago. Its primary unknowns, the material deformation map and the temperature field are governed by the material motion balance of momentum, i.e. the balance of material forces on the material manifold in the sense of Eshelby, and the balance of energy.

From a computational point of view, the material version of the balance of momentum is particularly attractive since it renders additional information without requiring the solution of a completely new system of equations. Rather, it can be understood as a mere postprocessing step once the spatial motion problem has been solved. Since the first numerical evaluation of the material force balance by Braun [4], the computational analysis of the material motion problem within the finite element framework has become a branch of active research. Herein, we shall adopt the so-called material force method as advocated by Steinmann [35], Steinmann et al. [38] and Denzer et al. [6] in the context of linear and nonlinear elastic fracture mechanics. Due to its computational efficiency, the material force method has been applied to a number of different problem classes such as thermomechanics by Shih et al. [31], tire mechanics by Govindjee [9], classical fracture mechanics by Müller et al. [26] and Müller and Maugin [25], biomechanics by Kuhl and Steinmann [15] or damage mechanics by Liebe et al. [17]. Since the resulting discrete material forces typically indicate a potential energy increase upon replacement of the material node point positions, spurious material forces can be utilized to improve the finite element mesh. To this end, Askes et al. [2,3] and Kuhl et al. [14] analyzed the staggered and the fully coupled solution of the spatial and the material motion balance of momentum introducing both, the spatial and the material motion map as primary unknowns. Within the present contribution, however, we shall restrict ourselves to a purely postprocessing-based analysis of the material motion problem.

In hyperelastic applications, the discrete material node point forces can essentially be computed as a function of the material motion momentum flux, i.e. the static or dynamic Eshelby stress tensor. Never-

theless, for the class of thermoelastic problems considered herein, an additional contribution in the material motion momentum source has to be taken into account. In the context of thermodynamics, this additional term can basically be expressed as a function of the temperature gradient and the entropy density. The elaboration of the influence of the temperature field on the material forces thus constitutes the main objective of the present work.

We begin by briefly reviewing the kinematic setting of the spatial and the material motion problem in Section 2. Next, we illustrate the fundamental balance equations characterizing a thermo-hyperelastic material behavior in Section 3. The residual statements of the balance of momentum and energy are then cast into their weak formats in Section 4 before their temporal and spatial discretization is carried out in Section 5. To illustrate the formal duality of the spatial and the material motion framework, we introduce both settings independently in each of the above-mentioned sections. Only at the end of each section, relations between the spatial and material motion quantities are pointed out. The features of the presented algorithmic framework are illustrated with the help of a number of classical examples from fracture mechanics in Section 6. The contribution ends with a final discussion in Section 7.

2. Kinematics

To introduce our notation, we shall briefly review the underlying geometrically nonlinear kinematics of the spatial and the material motion problem. While the classical spatial motion problem is based on the idea of following physical particles from a fixed material position $\boldsymbol{X}$ through the ambient space, the material motion problem essentially characterizes the movement of physical particles through the ambient material at fixed spatial position $\boldsymbol{x}$.

2.1. Spatial motion problem

Let $\mathscr{B}_0$ denote the material configuration occupied by the body of interest at time t_0. The spatial motion problem is thus characterized through the nonlinear spatial deformation map

$$\boldsymbol{x} = \boldsymbol{\varphi}(\boldsymbol{X}, t) : \mathscr{B}_0 \to \mathscr{B}_t \tag{1}$$

assigning the material placement $\boldsymbol{X} \in \mathscr{B}_0$ of a physical particle to its spatial placement $\boldsymbol{x} \in \mathscr{B}_t$, see Fig. 1. The related spatial deformation gradient $\boldsymbol{F}$

$$\boldsymbol{F} = \nabla_X \boldsymbol{\varphi}(\boldsymbol{X}, t) : T\mathscr{B}_0 \to T\mathscr{B}_t \tag{2}$$

defines the linear tangent map from the material tangent space $T\mathscr{B}_0$ to the tangent space $T\mathscr{B}_t$ while its Jacobian will be denoted as $J = \det \boldsymbol{F} > 0$. We shall introduce the right Cauchy–Green strain tensor $\boldsymbol{C} = \boldsymbol{F}^t \cdot \boldsymbol{g} \cdot \boldsymbol{F}$, i.e. the spatial motion pull back of the spatial metric $\boldsymbol{g}$ as a typical strain measure of the spatial motion problem. In what follows, the material time derivative of an arbitrary quantity $\{\bullet\}$ at fixed material placement $\boldsymbol{X}$ will be denoted as $D_t\{\bullet\} = \partial_t\{\bullet\}|_X$. Accordingly, the spatial velocity $\boldsymbol{v}$ can be introduced as the material time derivative of the spatial motion map as $\boldsymbol{v} = D_t\boldsymbol{\varphi}(\boldsymbol{X}, t)$. The gradient and the divergence of an arbitrary quantity $\{\bullet\}$ with respect to the material placement will be denoted as ∇_X and Div, respectively.

2.2. Material motion problem

Likewise, let $\mathscr{B}_t$ denote the spatial configuration occupied by the body of interest at time t. Guided by arguments of duality, we can introduce the material deformation map $\boldsymbol{\Phi}$

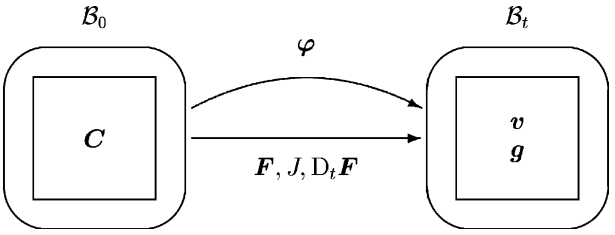

Fig. 1. Spatial motion problem: kinematics.

$$\boldsymbol{X} = \boldsymbol{\Phi}(\boldsymbol{X}, t) : \mathscr{B}_t \to \mathscr{B}_0 \tag{3}$$

defining the mapping of the spatial placement of a physical particle $\boldsymbol{x} \in \mathscr{B}_t$ to its material placement $\boldsymbol{X} \in \mathscr{B}_0$, see Fig. 2. Correspondingly, the material deformation gradient $\boldsymbol{f}$

$$\boldsymbol{f} = \nabla_x \boldsymbol{\Phi}(\boldsymbol{x}, t) : \quad T\mathscr{B}_t \to T\mathscr{B}_0 \tag{4}$$

defines the related linear tangent map from the spatial tangent space $T\mathscr{B}_t$ to the material tangent space $T\mathscr{B}_0$ with the related material Jacobian $j = \det \boldsymbol{f} > 0$. In complete analogy to the spatial motion case, we can introduce the material motion right Cauchy Green strain tensor $\boldsymbol{c} = \boldsymbol{f}^t \cdot \boldsymbol{G} \cdot \boldsymbol{f}$, i.e. the material motion pull back of the material metric $\boldsymbol{G}$. To clearly distinguish between the spatial and the material motion problem, we shall denote the spatial time derivative of a quantity $\{\bullet\}$ at fixed spatial placements $\boldsymbol{x}$ as $d_t\{\bullet\} = \partial_t\{\bullet\}|_x$. It defines the material velocity $\boldsymbol{V}$ as the spatial time derivative of the material motion map $\boldsymbol{V} = d_t \boldsymbol{\Phi}(\boldsymbol{x}, t)$. Moreover, let ∇_x and div denote the gradient and divergence of an arbitrary quantity $\{\bullet\}$ with respect to the spatial placement.

Remark 2.1 (*Spatial vs. material motion kinematics*). The spatial and the material motion problem are related through the identity maps in $\mathscr{B}_0$ and $\mathscr{B}_t$ while the corresponding deformation gradients are simply related via their inverses as $\boldsymbol{F}^{-1} = \boldsymbol{f}(\boldsymbol{\varphi}(\boldsymbol{X}, t), t)$ and $\boldsymbol{f}^{-1} = \boldsymbol{F}(\boldsymbol{\Phi}(\boldsymbol{x}, t), t)$. Moreover, the spatial and the material velocity are related via the following fundamental relations $\boldsymbol{V} = -\boldsymbol{f} \cdot \boldsymbol{v}$ and $\boldsymbol{v} = -\boldsymbol{F} \cdot \boldsymbol{V}$ which can be derived from the total differentials of the spatial and material identity map in a straightforward way, see e.g. Maugin [19] or Steinmann [37]. Recall, that the material and spatial time derivative of any scalar- or vector-valued function $\{\bullet\}$ are related through the Euler theorem as $D_t\{\bullet\} = d_t\{\bullet\} + \nabla_x\{\bullet\} \cdot \boldsymbol{v}$ and $d_t\{\bullet\} = D_t\{\bullet\} + \nabla_X\{\bullet\} \cdot \boldsymbol{V}$. Moreover, the material and the spatial time derivative of a volume specific scalar- or vector-valued function $\{\bullet\}_0 = \rho_0\{\bullet\}$ and $\{\bullet\}_t = \rho_t\{\bullet\}$ characterized in terms of the material and spatial density ρ_0 and ρ_t are related through the spatial and material motion version of Reynold's transport theorem as $jD_t\{\bullet\}_0 = d_t\{\bullet\}_t + \mathrm{div}(\{\bullet\}_t \otimes \boldsymbol{v})$ and $Jd_t\{\bullet\}_t = D_t\{\bullet\}_t + \mathrm{Div}(\{\bullet\}_0 \otimes \boldsymbol{V})$.

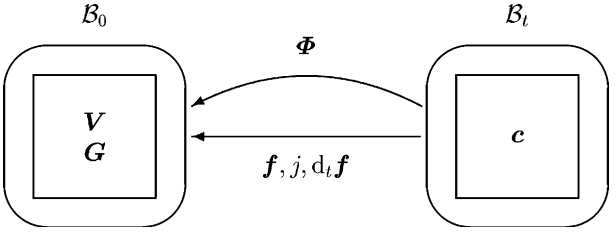

Fig. 2. Material motion problem: kinematics.

3. Thermo-hyperelasticity

The following section is devoted to the governing equations of thermo-hyperelasticity within the framework of rational thermodynamics as introduced by Truesdell and Toupin [40], Coleman and Noll [5] or Truesdell and Noll [39]. While the deformation problem is primarily governed by the balance of momentum, the temperature problem is characterized through the balance of energy. The latter can either be formulated in an entropy-based or in a more familiar temperature-based format. After illustrating the sets of equations in the spatial and the material motion setting, relations between the individual spatial and material quantities will be given.

3.1. Spatial motion problem

For the spatial motion problem, the balance of momentum balances the rate of change of the spatial momentum $\boldsymbol{p}_0 = \rho_0 \boldsymbol{g} \cdot \boldsymbol{v}$ which is nothing but the material velocity $\boldsymbol{v}$ weighted by the material density ρ_0 with the momentum flux $\boldsymbol{\Pi}^t$, i.e. the first Piola–Kirchhoff stress tensor, and the momentum source $\boldsymbol{b}_0$:

$$D_t \boldsymbol{p}_0 = \mathrm{Div}\, \boldsymbol{\Pi}^t + \boldsymbol{b}_0. \tag{5}$$

For the sake of duality, the momentum source $\boldsymbol{b}_0$ can be introduced as the sum of an external and an internal contribution, $\boldsymbol{b}_0 = \boldsymbol{b}_0^{\mathrm{ext}} + \boldsymbol{b}_0^{\mathrm{int}}$. However, it will turn out later on, that for the spatial motion problem, the internal contribution $\boldsymbol{b}_0^{\mathrm{int}}$ vanishes identically as $\boldsymbol{b}_0^{\mathrm{int}} = \boldsymbol{0}$. The second fundamental balance equation in thermomechanics is the balance of energy, which can be stated in the following entropy-based format:

$$\theta D_t S_0 = -\mathrm{Div}\, \boldsymbol{Q} + \mathcal{Z}_0 + \mathsf{D}_0 - \mathsf{D}_0^{\mathrm{con}}. \tag{6}$$

In the above equation, S_0 denotes the material entropy density while $\boldsymbol{Q}$ and $\mathcal{Z}_0$ are the material heat flux vector and the material heat source, respectively. Moreover, D_0 denotes the material dissipation power, which can be understood as the sum of a convective and a local part, as $\mathsf{D}_0 = \mathsf{D}_0^{\mathrm{con}} + \mathsf{D}_0^{\mathrm{loc}}$. Following the standard argumentation in classical rational thermodynamics, we shall assume the convective part $\mathsf{D}_0^{\mathrm{con}} \geqslant 0$ to be nonnegative throughout and the local part $\mathsf{D}_0^{\mathrm{loc}} = 0$ to vanish identically as

$$\mathsf{D}_0^{\mathrm{loc}} = \boldsymbol{\Pi}^t : D_t \boldsymbol{F} - \boldsymbol{v} \cdot \boldsymbol{b}_0^{\mathrm{int}} - D_t \Psi_0 - S_0 D_t \theta = 0, \quad \mathsf{D}_0^{\mathrm{con}} = -\boldsymbol{Q} \cdot \nabla_X \ln \theta \geqslant 0, \tag{7}$$

thus guaranteeing that $\mathsf{D}_0 \geqslant 0$. In what follows, we shall consider a hyperelastic material characterized through the free energy density $\Psi_0 = \Psi_0(\boldsymbol{F}, \theta; \boldsymbol{X})$ being a function of the spatial motion deformation gradient $\boldsymbol{F}$ and the absolute temperature θ with a possible explicit dependence of the material placement $\boldsymbol{X}$. The evaluation of the spatial motion version of the Clausius–Planck inequality $(7)_1$ with

$$\Psi_0 = \Psi_0(\boldsymbol{F}, \theta; \boldsymbol{X}), \quad D_t \Psi_0 = D_{\boldsymbol{F}} \Psi_0 : D_t \boldsymbol{F} + D_0 \Psi_0 D_t \theta, \tag{8}$$

thus renders the definition of the first Piola–Kirchhoff stress tensor $\boldsymbol{\Pi}^t$ and the material entropy density S_0 as thermodynamically conjugate variables to the spatial motion deformation gradient $\boldsymbol{F}$ and the absolute temperature θ. Moreover, it turns out that the internal forces $\boldsymbol{b}_0^{\mathrm{int}}$ of the spatial motion problem vanish identically, compare e.g. Steinmann [37]:

$$\boldsymbol{\Pi}^t = D_{\boldsymbol{F}} \Psi_0, \quad S_0 = -D_0 \Psi_0, \quad \boldsymbol{b}_0^{\mathrm{int}} = \boldsymbol{0}. \tag{9}$$

The material time derivative of the entropy density S_0 can thus be expressed in the following format, $D_t S_0 = D_0 S_0 D_t \theta - D_0 \boldsymbol{\Pi}^t : D_t \boldsymbol{F}$. With these results at hand, we can recast the entropy-based balance of energy (6) in its more familiar temperature-based format,

$$c_0 D_t \theta = -\mathrm{Div}\, \boldsymbol{Q} + \mathcal{Z}_0 + \mathcal{Z}_0^{\mathrm{mech}} \tag{10}$$

with the specific material heat capacity at constant deformation $c_0 = \theta D_0 S_0$ and the thermomechanical coupling term $\mathcal{Q}_0^{\text{mech}} = \theta D_0 \boldsymbol{\Pi}^t : D_t \boldsymbol{F}$ which is typically responsible for the so-called Gough–Joule effect.

3.2. Material motion problem

Conceptually speaking, the balance of momentum of the material motion problem follows from a complete projection of the classical momentum balance (5) onto the material manifold. It balances the time rate of change of the material motion momentum $\boldsymbol{P}_0 = \rho_0 \boldsymbol{C} \cdot \boldsymbol{V}$ with the material motion momentum flux $\boldsymbol{\pi}^t - T_t \boldsymbol{F}^t$ and momentum source $\mathbf{B}_t + \partial_{\boldsymbol{\Phi}} K_t$:

$$j D_t \boldsymbol{P}_0 = \operatorname{div}(\boldsymbol{\pi}^t - K_t \boldsymbol{F}^t) + \boldsymbol{B}_t + \partial_{\boldsymbol{\Phi}} K_t. \tag{11}$$

In the transient case, the classical static material momentum flux $\boldsymbol{\pi}^t$ has to be modified by the correction term $K_t \boldsymbol{F}^t$ in terms of the kinetic energy density $K_t = \rho_t \boldsymbol{V} \cdot \boldsymbol{C} \cdot \boldsymbol{V}/2$. Likewise, the material volume force $\boldsymbol{B}_t = \boldsymbol{B}_t^{\text{ext}} + \mathbf{B}_t^{\text{int}}$ which typically consists of an external and an internal contribution contains an additional transient term $\partial_{\boldsymbol{\Phi}} T_t$. Note that for the sake of duality, we prefer a formulation in terms of the two-point representation $\boldsymbol{\pi}^t$ of the classical Eshelby stress tensor $\boldsymbol{\Sigma}^t = J \boldsymbol{\pi}^t \cdot \boldsymbol{f}^t$, rather than working with the traditional Eshelby tensor $\boldsymbol{\Sigma}^t$ itself, see also Remark 3.1. The balance of energy of the material motion problem can be stated in the following entropy-based format,

$$j \theta D_t S_0 = -\operatorname{div} \boldsymbol{q} + \mathcal{Q}_t + \mathsf{D}_t - \mathsf{D}_t^{\text{con}} \tag{12}$$

with $\boldsymbol{q}$ and $\mathcal{Q}_t$ denoting the spatial heat flux vector and heat source, respectively. The spatial dissipation D_t consists of a convective and a local contribution $\mathsf{D}_t = \mathsf{D}_t^{\text{con}} + \mathsf{D}_t^{\text{loc}}$ with $\mathsf{D}_t^{\text{con}} \geqslant 0$ and $\mathsf{D}_t^{\text{loc}} = 0$ vanishing identically as

$$\mathsf{D}_t^{\text{loc}} = \boldsymbol{\pi}^t : d_t \boldsymbol{f} - \boldsymbol{V} \cdot \boldsymbol{B}_t^{\text{int}} - d_t \Psi_t - S_t D_t \theta = 0, \quad \mathsf{D}_t^{\text{con}} = -\boldsymbol{q} \cdot \nabla_x \ln \theta \geqslant 0, \tag{13}$$

such that $\mathsf{D}_t \geqslant 0$ is a priori guaranteed for the hyperelastic materials considered in the sequel. Next, we introduce the free energy density $\Psi_t = \Psi_t(\boldsymbol{f}, \theta, \boldsymbol{\Phi})$ as a function of the material motion deformation gradient $\boldsymbol{f}$, the absolute temperature θ and the material placement $\boldsymbol{\Phi}$. The evaluation of the material motion version of the Clausius–Planck inequality $(13)_1$ according to Steinmann [37] with

$$\Psi_t = \Psi_t(\boldsymbol{f}\ , \theta, \boldsymbol{\Phi}), \quad d_t \Psi_t = d_f \Psi_t : d_t \boldsymbol{f} + d_0 \Psi_t d_t \theta + d_{\boldsymbol{\Phi}} \Psi_t \cdot d_t \boldsymbol{\Phi}, \tag{14}$$

and $d_t \boldsymbol{\Phi} = \boldsymbol{V}$ renders the definition of the material motion momentum flux $\boldsymbol{\pi}^t$ as thermodynamically conjugate variable to the material motion deformation gradient $\boldsymbol{f}$, the entropy density S_0 as conjugate variable to the temperature θ and a definition of the internal forces $\boldsymbol{B}_t^{\text{int}}$ which are generally different from zero in the material setting:

$$\boldsymbol{\pi}^t = d_f \Psi_t, \quad S_t = -d_0 \Psi_t, \quad \boldsymbol{B}_t^{\text{int}} = S_t \nabla_X \theta - \partial_{\boldsymbol{\Phi}} \Psi_t. \tag{15}$$

Similar to the spatial motion problem, the balance of energy (12) can be cast into its more familiar temperature-based format

$$c_t D_t \theta = -\operatorname{div} \boldsymbol{q} + \mathcal{Q}_t + \mathcal{Q}_t^{\text{mech}} \tag{16}$$

by making use of the above-derived definitions.

Remark 3.1 (*Spatial vs. material quantities*). The material motion version of the balance of momentum (11) follows from a complete projection of its spatial motion counterpart (5) onto the material manifold through a premultiplication with $-j\boldsymbol{F}^t$.

$$-j\boldsymbol{F}^t \cdot D_t \boldsymbol{p}_0 = -j\boldsymbol{F}^t \cdot \operatorname{Div} \boldsymbol{\Pi}^t - j\boldsymbol{F}^t \cdot \boldsymbol{b}_0. \tag{17}$$

A closer evaluation of the left-hand side of the above equation reveals the following identity:

$$-j\boldsymbol{F}^t \cdot D_t\boldsymbol{p}_0 = jD_t[-\boldsymbol{F}^t \cdot \boldsymbol{p}_0] + \operatorname{div}(jT_0\boldsymbol{F}^t) - j\partial_{\boldsymbol{\Phi}}T_0. \tag{18}$$

Accordingly, the first term on the righthand side can be reformulated in the following form

$$-j\boldsymbol{F}^t \cdot \operatorname{Div}\boldsymbol{\Pi}^t = \operatorname{div}(-j\boldsymbol{F}^t \cdot \boldsymbol{\Pi}^t \cdot \boldsymbol{F}^t) + j\boldsymbol{\Pi}^t : \nabla_X\boldsymbol{F} \tag{19}$$

by making use of the kinematic compatibility condition $\nabla_X\boldsymbol{F}^t : \boldsymbol{\Pi}^t = \boldsymbol{\Pi}^t : \nabla_X\boldsymbol{F}$. Moreover, the last term can be expressed as $j\boldsymbol{\Pi}^t : \nabla_X\boldsymbol{F} = \operatorname{div}(j\Psi_0\boldsymbol{F}^t) - jD_0\Psi_0\nabla_X\theta - j\partial_{\boldsymbol{\Phi}}\Psi_0$ whereby $-D_0\Psi_0 = S_0$. When separating transient terms, flux and source terms, we can rewrite Eq. (17) in the following format:

$$jD_t[-\boldsymbol{F}^t \cdot \boldsymbol{p}_0] = \operatorname{div}(-j\boldsymbol{F}^t \cdot \boldsymbol{\Pi}^t \cdot \boldsymbol{F}^t + j[\Psi_0 - T_0]\boldsymbol{F}^t) - j\boldsymbol{F}^t \cdot \boldsymbol{b}_0 + jS_0\nabla_X\theta - j\partial_{\boldsymbol{\Phi}}[\Psi_0 - T_0]. \tag{20}$$

A comparison of Eqs. (11) and (20) reveals the following relations between the spatial and material motion momentum and the corresponding flux and source terms:

$$\begin{aligned}
\boldsymbol{P}_0 &= -\boldsymbol{F}^t \cdot \boldsymbol{p}_0, \\
\boldsymbol{\pi}^t &= -j\boldsymbol{F}^t \cdot \boldsymbol{\Pi}^t \cdot \boldsymbol{F}^t + j\Psi_0\boldsymbol{F}^t, \\
\boldsymbol{B}_t &= -j\boldsymbol{F}^t \cdot \boldsymbol{b}_0 + jS_0\nabla_X\theta - j\partial_{\boldsymbol{\Phi}}\Psi_0.
\end{aligned} \tag{21}$$

Recall that $J\boldsymbol{\pi}^t \cdot \boldsymbol{f}^t$ renders the classical Eshelby stress tensor which takes the typical energy momentum format as $\boldsymbol{\Sigma}^t = \Psi_0\boldsymbol{I} - \boldsymbol{F}^t \cdot \boldsymbol{\Pi}^t$. The related transformation formulae for the scalar- and vector-valued quantities of the balance of energy simply follow from the appropriate weighting with the Jacobian $c_t = jc_0$, $\mathcal{Q}_t = j\mathcal{Q}_0$, $\mathcal{Q}_t^{\text{mech}} = j\mathcal{Q}_0^{\text{mech}}$, $\mathsf{D}_t = j\mathsf{D}_0$ and from the corresponding Piola transform as $\boldsymbol{q} = j\boldsymbol{Q} \cdot \boldsymbol{f}^{-t}$.

4. Weak form

As a prerequisite for the finite element formulation that will be derived in Section 5, we shall reformulate the balance of momentum and energy in their weak format.

4.1. Spatial motion problem

The global residual statements of the balance of momentum (5) and the temperature-based version of the balance of energy (10) read

$$\begin{aligned}
\mathbf{r}^{\varphi}(\theta, \boldsymbol{\varphi}) &= \mathbf{f}^{\varphi}_{\text{dyn}} - \mathbf{f}^{\varphi}_{\text{sur}} - \mathbf{f}^{\varphi}_{\text{vol}} = \mathbf{0}, \\
\mathsf{r}^{0}(\theta, \boldsymbol{\varphi}) &= \mathsf{f}^{0}_{\text{dyn}} - \mathsf{f}^{0}_{\text{sur}} - \mathsf{f}^{0}_{\text{vol}} = 0,
\end{aligned} \tag{22}$$

whereby the dynamic, the surface and the volume contribution expand in the following expressions:

$$\begin{aligned}
\mathbf{f}^{\varphi}_{\text{dyn}} &= \int_{\mathscr{B}_0} D_t\boldsymbol{p}_0 \,\mathrm{d}V, \quad \mathbf{f}^{\varphi}_{\text{sur}} = \int_{\partial\mathscr{B}_0} \boldsymbol{\Pi}^t \cdot \boldsymbol{N} \,\mathrm{d}A, \quad \mathbf{f}^{\varphi}_{\text{vol}} = \int_{\mathscr{B}_0} \boldsymbol{b}_0 \,\mathrm{d}V, \\
\mathsf{f}^{0}_{\text{dyn}} &= \int_{\mathscr{B}_0} c_0 D_t\theta \,\mathrm{d}V, \quad \mathsf{f}^{0}_{\text{sur}} = \int_{\partial\mathscr{B}_0} -\boldsymbol{Q} \cdot \boldsymbol{N} \,\mathrm{d}A, \quad \mathsf{f}^{0}_{\text{vol}} = \int_{\mathscr{B}_0} \mathcal{Q}_0 + \mathcal{Q}_0^{\text{mech}} \,\mathrm{d}V.
\end{aligned} \tag{23}$$

The residual statements (22) are supplemented by appropriate boundary conditions for the mechanical and the thermal fields. For the deformation problem $(22)_1$, the boundary $\partial\mathscr{B}_0$ is decomposed into disjoint parts as $\partial\mathscr{B}_0^{\varphi} \cup \partial\mathscr{B}_0^{t} = \partial\mathscr{B}_0$ and $\partial\mathscr{B}_0^{\varphi} \cap \partial\mathscr{B}_0^{t} = \emptyset$. Correspondingly, for the temperature problem $(22)_2$, the equivalent decomposition renders the disjoint boundary contributions $\partial\mathscr{B}_0^{0} \cup \partial\mathscr{B}_0^{q} = \partial\mathscr{B}_0$ and $\partial\mathscr{B}_0^{0} \cap \partial\mathscr{B}_0^{q} = \emptyset$. Dirichlet boundary conditions are prescribed for the deformation $\boldsymbol{\varphi}$ and the temperature θ

on $\mathscr{B}_0^{\varphi}$ and $\mathscr{B}_0^{\theta}$, whereas Neumann boundary can be introduced for the momentum flux $\boldsymbol{\Pi}^t$ and the heat flux $\boldsymbol{Q}$ on $\partial\mathscr{B}_0^t$ and $\partial\mathscr{B}_0^q$ in terms of the outward normal $\boldsymbol{N}$:

$$\begin{aligned} &\boldsymbol{\varphi} = \overline{\boldsymbol{\varphi}} \text{ on } \partial\mathscr{B}_0^{\varphi}, \quad \boldsymbol{\Pi}^t \cdot \boldsymbol{N} = \overline{\boldsymbol{t}} \text{ on } \partial\mathscr{B}_0^t, \\ &\theta = \overline{\theta} \text{ on } \partial\mathscr{B}_0^{\theta}, \quad \boldsymbol{Q} \cdot \boldsymbol{N} = \overline{q} \text{ on } \partial\mathscr{B}_0^q. \end{aligned} \tag{24}$$

By testing the local residual statements corresponding to $(22)_1$ and $(22)_2$ and the related Neumann boundary conditions $(24)_2$ and $(24)_4$ with the vector- and scalar-valued test functions $\boldsymbol{w}$ and ϑ, respectively, we can derive the corresponding weak forms

$$\begin{aligned} &\mathsf{g}^{\varphi}(\boldsymbol{w};\theta,\boldsymbol{\varphi}) = \mathsf{w}^{\varphi}_{\text{dyn}} + \mathsf{w}^{\varphi}_{\text{int}} - \mathsf{w}^{\varphi}_{\text{sur}} - \mathsf{w}^{\varphi}_{\text{vol}} = 0 \quad \forall \boldsymbol{w} \text{ in } H_1^0(\mathscr{B}_0), \\ &\mathsf{g}^{\theta}(\vartheta;\theta,\boldsymbol{\varphi}) = \mathsf{w}^{\theta}_{\text{dyn}} + \mathsf{w}^{\theta}_{\text{int}} - \mathsf{w}^{\theta}_{\text{sur}} - \mathsf{w}^{\theta}_{\text{vol}} = 0 \quad \forall \vartheta \text{ in } H_1^0(\mathscr{B}_0) \end{aligned} \tag{25}$$

provided that the related fields fulfill the necessary smoothness and boundary assumptions. By interpreting the vector-valued test function $\boldsymbol{w}$ as the spatial virtual displacements $\delta\boldsymbol{\varphi}$, Eq. $(25)_1$ can be identified as the virtual work expression of the spatial motion problem with the dynamic, the internal, the surface and the volume parts of the virtual work given in the familiar form:

$$\begin{aligned} \mathsf{w}^{\varphi}_{\text{dyn}} &= \int_{\mathscr{B}_0} \boldsymbol{w} \cdot D_t \boldsymbol{p}_0 \,\mathrm{d}V, \qquad \mathsf{w}^{\varphi}_{\text{int}} = \int_{\mathscr{B}_0} \nabla_X \boldsymbol{w} : \boldsymbol{\Pi}^t \,\mathrm{d}V, \\ \mathsf{w}^{\varphi}_{\text{sur}} &= \int_{\partial\mathscr{B}_0^t} \boldsymbol{w} \cdot \boldsymbol{\Pi}^t \cdot \boldsymbol{N} \,\mathrm{d}A, \quad \mathsf{w}^{\varphi}_{\text{vol}} = \int_{\mathscr{B}_0} \boldsymbol{w} \cdot \boldsymbol{b}_0 \,\mathrm{d}V. \end{aligned} \tag{26}$$

Accordingly, the scalar-valued test function ϑ can be interpreted as the virtual temperature $\delta\theta$. The dynamic, the internal, the surface and the volume contribution to the virtual temperature problem thus expand into the following expressions:

$$\begin{aligned} \mathsf{w}^{\theta}_{\text{dyn}} &= \int_{\mathscr{B}_0} \vartheta c_0 D_t \theta \,\mathrm{d}V, \qquad \mathsf{w}^{\theta}_{\text{int}} = \int_{\mathscr{B}_0} -\nabla_X \vartheta \cdot \boldsymbol{Q} \,\mathrm{d}V, \\ \mathsf{w}^{\theta}_{\text{sur}} &= \int_{\partial\mathscr{B}_0^q} -\vartheta \boldsymbol{Q} \cdot \boldsymbol{N} \,\mathrm{d}A, \quad \mathsf{w}^{\theta}_{\text{vol}} = \int_{\mathscr{B}_0} \vartheta [\mathscr{Q}_0 + \mathscr{Q}_0^{\text{mech}}] \,\mathrm{d}V. \end{aligned} \tag{27}$$

4.2. Material motion problem

Guided by arguments of duality, the global residual statements of the balance of momentum and energy of the material motion problem can be introduced in complete analogy to their spatial motion counterparts:

$$\begin{aligned} \mathbf{R}^{\Phi} &= \mathbf{F}^{\Phi}_{\text{dyn}} - \mathbf{F}^{\Phi}_{\text{sur}} - \mathbf{F}^{\Phi}_{\text{vol}} = \mathbf{0}, \\ \mathsf{R}^{\theta} &= \mathsf{F}^{\theta}_{\text{dyn}} - \mathsf{F}^{\theta}_{\text{sur}} - \mathsf{F}^{\theta}_{\text{vol}} = 0. \end{aligned} \tag{28}$$

The dynamic, the surface and the internal contribution to both equations can be expressed in the following form:

$$\begin{aligned} \mathbf{F}^{\Phi}_{\text{dyn}} &= \int_{\mathscr{B}_t} j D_t \boldsymbol{P}_0 \,\mathrm{d}v, \quad \mathbf{F}^{\Phi}_{\text{sur}} = \int_{\partial\mathscr{B}_t} [\boldsymbol{\pi}^t - K_t \boldsymbol{F}^t] \cdot \boldsymbol{n} \,\mathrm{d}a, \quad \mathbf{F}^{\Phi}_{\text{vol}} = \int_{\mathscr{B}_t} \boldsymbol{B}_t + \partial_{\boldsymbol{\Phi}} K_t \,\mathrm{d}v, \\ \mathsf{F}^{\theta}_{\text{dyn}} &= \int_{\mathscr{B}_t} c_t D_t \theta \,\mathrm{d}v, \quad \mathsf{F}^{\theta}_{\text{sur}} = \int_{\partial\mathscr{B}_t} -\boldsymbol{q} \cdot \boldsymbol{n} \,\mathrm{d}a, \qquad \mathsf{F}^{\theta}_{\text{vol}} = \int_{\mathscr{B}_t} \mathscr{Q}_t + \mathscr{Q}_t^{\text{mech}} \,\mathrm{d}v. \end{aligned} \tag{29}$$

Next, Dirichlet and Neumann boundary conditions can be defined for the material motion problem to illustrate the formal duality with the spatial motion problem. For the balance of momentum $(28)_1$, the

corresponding parts of the boundary will be introduced as $\partial\mathscr{B}_t^{\Phi} \cup \partial\mathscr{B}_t^{T} = \partial\mathscr{B}_t$ and $\partial\mathscr{B}_t^{\Phi} \cap \partial\mathscr{B}_t^{T} = \emptyset$ while for the balance of energy $(28)_2$, they read $\partial\mathscr{B}_t^{0} \cup \partial\mathscr{B}_t^{Q} = \partial\mathscr{B}_t$ and $\partial\mathscr{B}_t^{0} \cap \partial\mathscr{B}_t^{Q} = \emptyset$. Accordingly, the corresponding boundary conditions can be expressed in the following form:

$$\begin{aligned} \boldsymbol{\Phi} &= \overline{\boldsymbol{\Phi}} \text{ on } \partial\mathscr{B}_t^{\Phi}, \quad [\boldsymbol{\pi}^t - K_t \boldsymbol{F}^t] \cdot \boldsymbol{n} = \overline{\boldsymbol{T}} \text{ on } \partial\mathscr{B}_t^{T}, \\ \theta &= \overline{\theta} \text{ on } \partial\mathscr{B}_t^{0}, \quad \boldsymbol{q} \cdot \boldsymbol{n} = \overline{Q} \text{ on } \partial\mathscr{B}_t^{q}. \end{aligned} \tag{30}$$

By testing the pointwise statements of the material momentum and energy balance and the related Neumann boundary conditions with the vector- and scalar-valued test functions $\boldsymbol{W}$ and ϑ, we obtain the weak forms of the material motion problem:

$$\begin{aligned} \mathsf{G}^{\Phi}(\boldsymbol{W}; \theta, \boldsymbol{\Phi}) &= \mathsf{W}^{\Phi}_{\text{dyn}} + \mathsf{W}^{\Phi}_{\text{int}} - \mathsf{W}^{\Phi}_{\text{sur}} - \mathsf{W}^{\Phi}_{\text{vol}} = 0 \quad \forall \boldsymbol{W} \text{ in } H^0_1(\mathscr{B}_t), \\ \mathsf{G}^{0}(\vartheta; \theta, \boldsymbol{\Phi}) &= \mathsf{W}^{0}_{\text{dyn}} + \mathsf{W}^{0}_{\text{int}} - \mathsf{W}^{0}_{\text{sur}} - \mathsf{W}^{0}_{\text{vol}} = 0 \quad \forall \vartheta \text{ in } H^0_1(\mathscr{B}_t). \end{aligned} \tag{31}$$

Note, that by interpreting the test function $\boldsymbol{W}$ as the material virtual displacement $\boldsymbol{W} = \delta\boldsymbol{\Phi}$, Eq. $(31)_1$ can be interpreted as the material counterpart of the classical virtual work expression $(25)_1$. Accordingly, $\mathsf{W}^{\Phi}_{\text{dyn}}$ and $\mathsf{W}^{\Phi}_{\text{int}}$ denote the dynamic and the internal virtual work, while $\mathsf{W}^{\Phi}_{\text{sur}}$ and $\mathsf{W}^{\Phi}_{\text{vol}}$ are the corresponding surface and volume contributions:

$$\begin{aligned} \mathsf{W}^{\Phi}_{\text{dyn}} &= \int_{\mathscr{B}_t} \boldsymbol{W} \cdot j D_t \boldsymbol{P}_0 \, \mathrm{d}v, & \mathsf{W}^{\Phi}_{\text{int}} &= \int_{\mathscr{B}_t} \nabla_x \boldsymbol{W} : [\boldsymbol{\pi}^t - K_t \boldsymbol{F}^t] \, \mathrm{d}v, \\ \mathsf{W}^{\Phi}_{\text{sur}} &= \int_{\partial\mathscr{B}_t^{T}} \boldsymbol{W} \cdot [\boldsymbol{\pi}^t - K_t \boldsymbol{F}^t] \cdot \boldsymbol{n} \, \mathrm{d}a, & \mathsf{W}^{\Phi}_{\text{vol}} &= \int_{\mathscr{B}_t} \boldsymbol{W} \cdot [\boldsymbol{B}_t + \partial_{\boldsymbol{\Phi}} K_t] \, \mathrm{d}v. \end{aligned} \tag{32}$$

Furthermore, the dynamic, the internal, the surface and the volume contribution to the weak form of the energy balance $(31)_2$ expand into the following formats:

$$\begin{aligned} \mathsf{W}^{0}_{\text{dyn}} &= \int_{\mathscr{B}_t} \vartheta c_t D_t \theta \, \mathrm{d}v, & \mathsf{W}^{0}_{\text{int}} &= \int_{\mathscr{B}_t} -\nabla_x \vartheta \cdot \boldsymbol{q} \, \mathrm{d}v, \\ \mathsf{W}^{0}_{\text{sur}} &= \int_{\partial\mathscr{B}_t^{Q}} -\vartheta \boldsymbol{q} \cdot \boldsymbol{n} \, \mathrm{d}a, & \mathsf{W}^{0}_{\text{vol}} &= \int_{\mathscr{B}_t} \vartheta [\mathscr{Q}_t + \mathscr{Q}_t^{\text{mech}}] \, \mathrm{d}v. \end{aligned} \tag{33}$$

Remark 4.1 (*Spatial vs. material test functions*). While the scalar-valued test function ϑ testing the balance of energy is identical for the spatial and the material motion problem, the vector-valued test functions $\boldsymbol{w}$ and $\boldsymbol{W}$ are related by the fundamental relations $\boldsymbol{w} = -\boldsymbol{W} \cdot \boldsymbol{F}^t$ and $\boldsymbol{W} = -\boldsymbol{w} \cdot \boldsymbol{f}^t$ which can be verified easily by transforming the virtual work statements of the spatial and the material motion problem $(25)_2$ and $(31)_2$ into one another.

Remark 4.2 (*Spatial and material forces*). Note, that Eqs. $(23)_1$ define the different contributions to the spatial forces $\mathbf{f}^{\varphi}$ representing the traditional forces in the sense of Newton. These are generated by variations relative to the ambient space at fixed material position $\boldsymbol{X}$. On the contrary, Eqs. $(29)_1$ define material forces $\mathbf{F}^{\Phi}$ in the sense of Eshelby which are generated by variations relative to the ambient material at fixed spatial position $\boldsymbol{x}$. These material forces represent important measures in the mechanics of material inhomogeneities.

Remark 4.3 (*Material force method*). Recall, that for the spatial motion problem, the surface and the volume contributions to the weak forms (25), namely $\mathsf{w}^{\varphi}_{\text{sur}}$ and $\mathsf{w}^{\varphi}_{\text{vol}}$ for the deformation problem and $\mathsf{w}^{0}_{\text{sur}}$ and $\mathsf{w}^{0}_{\text{vol}}$ for the temperature problem typically represent given quantities which define the primary unknowns $\boldsymbol{\varphi}$ and θ. Once the spatial motion problem is solved, the dynamic term $\mathsf{W}^{\Phi}_{\text{dyn}}$, the internal virtual work $\mathsf{W}^{\Phi}_{\text{int}}$ and the volume contribution $\mathsf{W}^{\Phi}_{\text{vol}}$ to the material momentum balance can be computed directly.

Correspondingly, the material surface forces $\mathbf{F}^{\Phi}_{\text{sur}}$ furnish the primary unknown of the material motion problem. Their numerical evaluation has been advocated as material force method by Steinmann et al. [38], see also Denzer et al. [6], Kuhl and Steinmann [15] or Liebe et al. [17].

5. Discretization

Eqs. (25) and (31) define the weak forms of the initial boundary value problem of thermo-hyperelasticity for the spatial and the material motion problem. Traditionally, these equations are first discretized in time, typically with finite difference schemes, before a spatial discretization with the finite element method can be carried out. To this end, consider a partition of the time interval of interest $\mathscr{T}$

$$\mathscr{T} = \bigcup_{n=0}^{n_{\text{step}}-1} [t_n, t_{n+1}], \tag{34}$$

and focus on the typical subinterval $[t_n, t_{n+1}]$ whereby $\Delta t = t_{n+1} - t_n$ denotes the corresponding actual time increment. Assume, that the primary unknowns, either the spatial or the material deformation $\boldsymbol{\varphi}_n$ or $\boldsymbol{\Phi}_n$ and the temperature θ_n and all derivable quantities are known at time t_n. Without loss of generality, we apply the classical Euler backward integration scheme to advance the solution in time from the known time step t_n to the actual time step t_{n+1}, keeping in mind that for the time integration of the second order balance of momentum, energy conserving integration algorithms would certainly be a more appropriate choice. The first order material time derivatives of the spatial and the material momentum $\boldsymbol{p}_0$ and $\boldsymbol{P}_0$ and the temperature θ can thus be approximated in the following way:

$$\begin{aligned} D_t\boldsymbol{p}_0 &= \frac{1}{\Delta t}[\boldsymbol{p}_{0n+1} - \boldsymbol{p}_{0n}], \\ D_t\boldsymbol{P}_0 &= \frac{1}{\Delta t}[\boldsymbol{P}_{0n+1} - \boldsymbol{P}_{0n}], \\ D_t\theta &= \frac{1}{\Delta t}[\theta_{n+1} - \theta_n]. \end{aligned} \tag{35}$$

Moreover, the governing equations can now be reformulated in terms of the unknown spatial deformation $\boldsymbol{\varphi}_{n+1}$ and the temperature θ_{n+1} at time t_{n+1} for the spatial motion problem

$$\begin{aligned} \mathsf{g}^{\varphi}_{n+1}(\boldsymbol{w}; \theta_{n+1}, \boldsymbol{\varphi}_{n+1}) &= \mathsf{w}^{\varphi}_{\text{dyn}} + \mathsf{w}^{\varphi}_{\text{int}} - \mathsf{w}^{\varphi}_{\text{sur}} - \mathsf{w}^{\varphi}_{\text{vol}} = 0 \quad \forall \boldsymbol{w} \text{ in } H^0_1(\mathscr{B}_0), \\ \mathsf{g}^{\vartheta}_{n+1}(\vartheta; \theta_{n+1}, \boldsymbol{\varphi}_{n+1}) &= \mathsf{w}^{\vartheta}_{\text{dyn}} + \mathsf{w}^{\vartheta}_{\text{int}} - \mathsf{w}^{\vartheta}_{\text{sur}} - \mathsf{w}^{\vartheta}_{\text{vol}} = 0 \quad \forall \vartheta \text{ in } H^0_1(\mathscr{B}_0), \end{aligned} \tag{36}$$

and in terms of the material deformation $\boldsymbol{\Phi}_{n+1}$ and the temperature θ_{n+1} for the material motion problem:

$$\begin{aligned} \mathsf{G}^{\vartheta}_{n+1}(\vartheta; \theta_{n+1}, \boldsymbol{\Phi}_{n+1}) &= \mathsf{W}^{\vartheta}_{\text{dyn}} + \mathsf{W}^{\vartheta}_{\text{int}} - \mathsf{W}^{\vartheta}_{\text{sur}} - \mathsf{W}^{\vartheta}_{\text{vol}} = 0 \quad \forall \vartheta \text{ in } H^0_1(\mathscr{B}_t), \\ \mathsf{G}^{\boldsymbol{\Phi}}_{n+1}(\boldsymbol{W}; \theta_{n+1}, \boldsymbol{\Phi}_{n+1}) &= \mathsf{W}^{\boldsymbol{\Phi}}_{\text{dyn}} + \mathsf{W}^{\boldsymbol{\Phi}}_{\text{int}} - \mathsf{W}^{\boldsymbol{\Phi}}_{\text{sur}} - \mathsf{W}^{\boldsymbol{\Phi}}_{\text{vol}} = 0 \quad \forall \boldsymbol{W} \text{ in } H^0_1(\mathscr{B}_t). \end{aligned} \tag{37}$$

The semi-discrete weak forms (36) and (37) lend themselves readily for the spatial discretization within the finite element framework which be illustrated in the following sections.

5.1. Spatial motion problem

Let $\mathscr{B}_0$ denote the region occupied by the reference configuration of a solid continuum body at time $t = t_0$. In the spirit of the finite element method, this reference domain is discretized in n_{el} elements $\mathscr{B}^e_0$. The underlying geometry $\boldsymbol{X}$ is interpolated elementwise by the shape functions N^i_X in terms of the discrete node point positions $\boldsymbol{X}_i$ of the $i = 1 \ldots n_{\text{en}}$ element nodes:

$$\mathscr{B}_0 = \bigcup_{e=1}^{n_{\text{el}}} \mathscr{B}_0^e, \quad \boldsymbol{X}^h|_{\mathscr{B}_0^e} = \sum_{i=1}^{n_{\text{en}}} N_X^i \boldsymbol{X}_i. \tag{38}$$

According to the isoparametric concept, we shall interpolate the unknowns $\boldsymbol{\varphi}$ and θ on the element level with the same shape functions N_φ^i and N_0^j as the element geometry $\boldsymbol{X}$. In the spirit of the classical Bubnov–Galerkin technique, similar shape functions are applied to interpolate the test functions $\boldsymbol{w}$ and ϑ:

$$\begin{aligned} \boldsymbol{w}^h|_{\mathscr{B}_0^e} &= \sum_{i=1}^{n_{\text{en}}} N_\varphi^i \boldsymbol{w}_i \in H_1^0(\mathscr{B}_0), \quad \boldsymbol{\varphi}^h|_{\mathscr{B}_0^e} = \sum_{k=1}^{n_{\text{en}}} N_\varphi^k \boldsymbol{\varphi}_k \in H_1(\mathscr{B}_0), \\ \vartheta^h|_{\mathscr{B}_0^e} &= \sum_{j=1}^{n_{\text{en}}} N_0^j \vartheta_j \in H_1^0(\mathscr{B}_0), \quad \theta^h|_{\mathscr{B}_0^e} = \sum_{l=1}^{n_{\text{en}}} N_0^l \theta_l \in H_1(\mathscr{B}_0). \end{aligned} \tag{39}$$

The related gradients of the test functions $\nabla_X \boldsymbol{w}^h$ and $\nabla_X \vartheta^h$ and the gradients of the primary unknowns $\nabla_X \boldsymbol{\varphi}^h$ and $\nabla_X \theta^h$ thus take the following elementwise interpolation:

$$\begin{aligned} \nabla_X \boldsymbol{w}^h|_{\mathscr{B}_0^e} &= \sum_{i=1}^{n_{\text{en}}} \boldsymbol{w}_i \otimes \nabla_X N_\varphi^i, \quad \nabla_X \boldsymbol{\varphi}^h|_{\mathscr{B}_0^e} = \sum_{k=1}^{n_{\text{en}}} \boldsymbol{\varphi}_k \otimes \nabla_X N_\varphi^k, \\ \nabla_X \vartheta^h|_{\mathscr{B}_0^e} &= \sum_{j=1}^{n_{\text{en}}} \vartheta_j \nabla_X N_0^j, \qquad \nabla_X \theta^h|_{\mathscr{B}_0^e} = \sum_{l=1}^{n_{\text{en}}} \theta_l \nabla_X N_0^l. \end{aligned} \tag{40}$$

Recall, that herein, $\nabla_X \boldsymbol{\varphi}^h|_{\mathscr{B}_0^e}$ denotes the discrete spatial deformation gradient as $\boldsymbol{F}^h|_{\mathscr{B}_0^e} = \nabla_X \boldsymbol{\varphi}^h|_{\mathscr{B}_0^e}$. With the above-suggested discretizations in time and space, the fully discrete algorithmic balance of momentum and energy of the spatial motion problem take the following format:

$$\begin{aligned} \mathbf{r}_I^{\varphi h}(\theta_{n+1}^h, \boldsymbol{\varphi}_{n+1}^h) &= \mathbf{f}_{\text{dyn}I}^{\varphi h} + \mathbf{f}_{\text{int}I}^{\varphi h} - \mathbf{f}_{\text{sur}I}^{\varphi h} - \mathbf{f}_{\text{vol}I}^{\varphi h} = \mathbf{0} \quad \forall I = 1, n_{\text{np}}, \\ \mathrm{r}_J^{0h}(\theta_{n+1}^h, \boldsymbol{\varphi}_{n+1}^h) &= \mathrm{f}_{\text{dyn}J}^{0h} + \mathrm{f}_{\text{int}J}^{0h} - \mathrm{f}_{\text{sur}J}^{0h} - \mathrm{f}_{\text{vol}J}^{0h} = 0 \quad \forall J = 1, n_{\text{np}}. \end{aligned} \tag{41}$$

Herein, the discrete inertia forces, the internal forces, the surface forces and the volume forces can be expressed as

$$\begin{aligned} \mathbf{f}_{\text{dyn}I}^{\varphi h} &= \mathop{\mathbf{A}}_{e=1}^{n_{\text{el}}} \int_{\mathscr{B}_0^e} N_\varphi^i \frac{\boldsymbol{p}_{0n+1} - \boldsymbol{p}_{0n}}{\Delta t} \mathrm{d}V, \quad \mathbf{f}_{\text{int}I}^{\varphi h} = \mathop{\mathbf{A}}_{e=1}^{n_{\text{el}}} \int_{\mathscr{B}_0^e} \nabla_X N_\varphi^i \cdot \boldsymbol{\Pi}_{n+1} \mathrm{d}V, \\ \mathbf{f}_{\text{sur}I}^{0h} &= \mathop{\mathbf{A}}_{e=1}^{n_{\text{el}}} \int_{\partial \mathscr{B}_0^{te}} N_0^i \bar{\boldsymbol{t}}_{n+1} \mathrm{d}A, \qquad \mathbf{f}_{\text{vol}I}^{0h} = \mathop{\mathbf{A}}_{e=1}^{n_{\text{el}}} \int_{\mathscr{B}_0^e} N_0^i \boldsymbol{b}_{0n+1} \mathrm{d}V, \end{aligned} \tag{42}$$

while the dynamic, the internal, the surface and the volume contribution of the balance of energy expand into the following expressions:

$$\begin{aligned} \mathrm{f}_{\text{dyn}J}^{0h} &= \mathop{\mathbf{A}}_{e=1}^{n_{\text{el}}} \int_{\mathscr{B}_0^e} N_0^j c_0 \frac{\theta_{n+1} - \theta_n}{\Delta t} \mathrm{d}V, \quad \mathrm{f}_{\text{int}J}^{0h} = \mathop{\mathbf{A}}_{e=1}^{n_{\text{el}}} \int_{\mathscr{B}_0^e} \nabla_X N_0^j \cdot \boldsymbol{Q}_{n+1} \mathrm{d}V, \\ \mathrm{f}_{\text{sur}J}^{0h} &= \mathop{\mathbf{A}}_{e=1}^{n_{\text{el}}} \int_{\partial \mathscr{B}_0^{qe}} -N_0^j \bar{q}_{n+1} \mathrm{d}A, \qquad \mathrm{f}_{\text{vol}J}^{0h} = \mathop{\mathbf{A}}_{e=1}^{n_{\text{el}}} \int_{\mathscr{B}_0^e} N_0^j [\mathscr{Q}_{0n+1} + \mathscr{Q}_{0n+1}^{\text{mech}}] \mathrm{d}V. \end{aligned} \tag{43}$$

In the above definitions, the operator $\mathbf{A}$ denotes the assembly over all $e = 1, n_{\text{el}}$ element contributions at the $i, j = 1, n_{\text{en}}$ element nodes to the global node point vectors at all $I, J = 1, n_{\text{np}}$ global node points. Eqs. (41) thus represent the coupled nonlinear set of governing equations which is suggested to be solved in a monolithic sense. The corresponding solution procedure in terms of the incremental iterative Newton–Raphson scheme is illustrated in the Appendix A. Recall, that the discrete spatial surface forces acting on the global node points can be calculated as

$$\mathbf{f}^{\varphi h}_{\mathrm{sur}I} = \mathop{\mathsf{A}}_{e=1}^{n_{\mathrm{el}}} \int_{\mathscr{B}^e_0} N^i_\varphi \frac{\boldsymbol{p}_{0n+1} - \boldsymbol{p}_{0n}}{\Delta t} + \nabla_X N^i_\varphi \cdot \boldsymbol{\Pi}_{n+1} - N^i_\varphi \boldsymbol{b}_{0n+1}\, \mathrm{d}V, \tag{44}$$

and are thus energetically conjugate to spatial variations of the node point positions.

5.2. Material motion problem

In complete analogy, we can discretize the domain of interest $\mathscr{B}_t$ in n_{el} elements $\mathscr{B}^e_t$ for the material motion problem. Correspondingly, the geometry $\boldsymbol{x}$ of each element is interpolated from the $i = 1 \ldots n_{\mathrm{en}}$ node point positions $\boldsymbol{x}_i$ by the shape functions N^i_x:

$$\mathscr{B}_t = \bigcup_{e=1}^{n_{\mathrm{el}}} \mathscr{B}^e_t, \quad \boldsymbol{x}^h|_{\mathscr{B}^e_t} = \sum_{i=1}^{n_{\mathrm{en}}} N^i_x \boldsymbol{x}_i. \tag{45}$$

By making use of the isoparametric concept, we shall interpolate the primary unknowns $\boldsymbol{\Phi}$ and θ with the same shape functions N^i_Φ and N^j_0 as the element geometry $\boldsymbol{x}$. Moreover, the test functions $\boldsymbol{W}$ and ϑ are discretized with the same shape functions N^i_Φ and N^j_0:

$$\begin{aligned} \boldsymbol{W}^h|_{\mathscr{B}^e_t} &= \sum_{i=1}^{n_{\mathrm{en}}} N^i_\Phi \boldsymbol{W}_i \in H^0_1(\mathscr{B}_t), \quad \boldsymbol{\Phi}^h|_{\mathscr{B}^e_t} = \sum_{k=1}^{n_{\mathrm{en}}} N^k_\Phi \boldsymbol{\Phi}_k \in H_1(\mathscr{B}_t), \\ \vartheta^h|_{\mathscr{B}^e_t} &= \sum_{j=1}^{n_{\mathrm{en}}} N^j_0 \vartheta_j \in H^0_1(\mathscr{B}_t), \qquad \theta^h|_{\mathscr{B}^e_t} = \sum_{l=1}^{n_{\mathrm{en}}} N^l_0 \theta_l \in_1 (\mathscr{B}_t). \end{aligned} \tag{46}$$

Accordingly, the discretization of the gradients of the test functions $\nabla_x \boldsymbol{W}^h$ and $\nabla_x \vartheta^h$ and the gradients of the primary unknowns $\nabla_x \boldsymbol{\Phi}^h$ and $\nabla_x \theta^h$ takes the following representation:

$$\begin{aligned} \nabla_x \boldsymbol{W}^h|_{\mathscr{B}^e_t} &= \sum_{i=1}^{n_{\mathrm{en}}} \boldsymbol{w}_i \otimes \nabla_x N^i_\Phi, \quad \nabla_x \boldsymbol{\Phi}^h|_{\mathscr{B}^e_t} = \sum_{k=1}^{n_{\mathrm{en}}} \boldsymbol{\Phi}_k \otimes \nabla_x N^k_\Phi, \\ \nabla_x \vartheta^h|_{\mathscr{B}^e_t} &= \sum_{j=1}^{n_{\mathrm{en}}} \vartheta_j \nabla_x N^j_0, \qquad \nabla_x \theta^h|_{\mathscr{B}^e_t} = \sum_{l=1}^{n_{\mathrm{en}}} \theta_l \nabla_x N^l_0. \end{aligned} \tag{47}$$

Herein, $\nabla_x \boldsymbol{\Phi}^h$ denotes the discrete material deformation gradient $\boldsymbol{f}^h|_{\mathscr{B}^e_t} = \nabla_x \boldsymbol{\Phi}^h|_{\mathscr{B}^e_t}$. Consequently, the discrete algorithmic balance of momentum and energy, the material motion counterparts of Eqs. (41), take the following representations:

$$\begin{aligned} \mathbf{R}^{\Phi h}_I(\theta^h_{n+1}, \boldsymbol{\Phi}^h_{n+1}) &= \mathbf{F}^{\Phi h}_{\mathrm{dyn}I} + \mathbf{F}^{\Phi h}_{\mathrm{int}I} - \mathbf{F}^{\Phi h}_{\mathrm{sur}I} - \mathbf{F}^{\Phi h}_{\mathrm{vol}I} = \mathbf{0} \quad \forall I = 1, n_{\mathrm{np}}, \\ \mathsf{R}^{0h}_J(\theta^h_{n+1}, \boldsymbol{\Phi}^h_{n+1}) &= \mathsf{F}^{0h}_{\mathrm{dyn}J} + \mathsf{F}^{0h}_{\mathrm{int}J} - \mathsf{F}^{0h}_{\mathrm{sur}J} - \mathsf{F}^{0h}_{\mathrm{vol}J} = 0 \quad \forall J = 1, n_{\mathrm{np}}. \end{aligned} \tag{48}$$

The discrete material inertia forces, the internal forces, the surface forces and the volume forces can be expressed as

$$\begin{aligned} \mathbf{F}^{\varphi h}_{\mathrm{dyn}I} &= \mathop{\mathsf{A}}_{e=1}^{n_{\mathrm{el}}} \int_{\mathscr{B}^e_t} N^i_\Phi j \frac{\boldsymbol{P}_{0n+1} - \boldsymbol{P}_{0n}}{\Delta t}\, \mathrm{d}v, \quad \mathbf{F}^{\varphi h}_{\mathrm{int}I} = \mathop{\mathsf{A}}_{e=1}^{n_{\mathrm{el}}} \int_{\mathscr{B}^e_t} \nabla_x N^i_\Phi \cdot [\boldsymbol{\pi} - K_t \boldsymbol{F}]_{n+1}\, \mathrm{d}v, \\ \mathbf{F}^{\varphi h}_{\mathrm{sur}I} &= \mathop{\mathsf{A}}_{e=1}^{n_{\mathrm{el}}} \int_{\partial \mathscr{B}^{Te}_t} N^i_\Phi \overline{\boldsymbol{T}}_{n+1}\, \mathrm{d}a, \qquad \mathbf{F}^{\varphi h}_{\mathrm{vol}I} = \mathop{\mathsf{A}}_{e=1}^{n_{\mathrm{el}}} \int_{\mathscr{B}^e_t} N^i_\Phi [\boldsymbol{B}_t + \partial_{\boldsymbol{\Phi}} K_t]_{n+1}\, \mathrm{d}v, \end{aligned} \tag{49}$$

while the dynamic, the internal, the surface and the volume contribution of the energy balance take the following format:

$$\begin{aligned} \mathsf{F}^{0h}_{\mathrm{dyn}J} &= \mathop{\mathsf{A}}_{e=1}^{n_{\mathrm{el}}} \int_{\mathscr{B}^e_t} N^j_0 c_t \frac{\theta_{n+1}-\theta_n}{\Delta t}\,\mathrm{d}v, \quad \mathsf{F}^{0h}_{\mathrm{int}J} = \mathop{\mathsf{A}}_{e=1}^{n_{\mathrm{el}}} \int_{\mathscr{B}^e_t} \nabla_x N^j_0 \cdot \boldsymbol{q}_{n+1}\,\mathrm{d}v, \\ \mathsf{F}^{0h}_{\mathrm{sur}J} &= \mathop{\mathsf{A}}_{e=1}^{n_{\mathrm{el}}} \int_{\partial\mathscr{B}^{Qe}_t} N^j_0 \overline{Q}_{tn+1}\,\mathrm{d}a, \qquad \mathsf{F}^{0h}_{\mathrm{vol}J} = \mathop{\mathsf{A}}_{e=1}^{n_{\mathrm{el}}} \int_{\mathscr{B}^e_t} N^j_0 [\mathscr{Q}_{tn+1} + \mathscr{Q}^{\mathrm{mech}}_{tn+1}]\,\mathrm{d}v. \end{aligned} \tag{50}$$

As a fundamental difference to the spatial motion problem, the Neumann boundary conditions of the material motion problem cannot be considered as given input data. Correspondingly, the discrete material forces acting on the global node points can only be computed in a post processing calculation once the spatial motion problem has been solved. Their definition parallels the definition of the discrete surface forces of the spatial motion problem given in Eq. (44). The discrete material surface forces

$$\mathsf{F}^{\varphi h}_{\mathrm{sur}I} = \mathop{\mathsf{A}}_{e=1}^{n_{\mathrm{el}}} \int_{\mathscr{B}^e_t} N^i_{\boldsymbol{\Phi}} j \frac{\boldsymbol{P}_{0n+1}-\boldsymbol{P}_{0n}}{\Delta t} + \nabla_x N^i_{\boldsymbol{\Phi}} \cdot [\boldsymbol{\pi} - K_t \boldsymbol{F}]_{n+1} - N^i_{\boldsymbol{\Phi}} [\boldsymbol{B}_t + \partial_{\boldsymbol{\Phi}} K_t]_{n+1}\,\mathrm{d}v \tag{51}$$

are thus energetically conjugate to material variations of the node point positions. They are readily computable once the solution to the spatial motion problem has been determined.

Remark 5.1 (*Transient terms in the residuals*). Coupled thermo-mechanical problems tend to involve time scales which typically differ by orders of magnitude. Rather than circumventing the problem of potentially ill-conditioned system matrices by making use of staggered solution techniques, we shall consider the balance of momentum $(41)_1$ or $(48)_1$ in a quasi-static sense in the sequel. In other words, the dynamic contributions which manifest themselves in the $N^j_\varphi[\boldsymbol{p}_{0n+1}-\boldsymbol{p}_{0n}]/\Delta t$ term of Eq. $(42)_1$ and in the $N^j_{\boldsymbol{\Phi}} j[\boldsymbol{P}_{0n+1}-\boldsymbol{P}_{0n}]/\Delta t$ term of Eq. $(49)_1$ are assumed to be negligible. Moreover, the dynamic correction to the material motion momentum flux and source, i.e. the $-K_t\boldsymbol{F}^t$ and the $\partial_{\boldsymbol{\Phi}} K_t$ term in Eq. $(49)_2$ and $(49)_4$, vanish identically in the quasi-static case. If the transient terms in the balance of spatial and material momentum cannot be neglected, we recommend the use of energy conserving time integration schemes rather than the dissipative integration algorithms of the Euler family, at least for the time integration of the second order equations.

Remark 5.2 (*Spatial vs. material quantities*). For the class of quasi-static problems considered in the sequel, the discrete momentum flux $\boldsymbol{\pi}^t_{n+1}$, and the corresponding momentum source $\boldsymbol{B}_{tn+1}$ that are essentially needed to compute the discrete material node point forces defined in Eq. (51) are related to their spatial motion counterparts $\boldsymbol{\Pi}^t_{n+1}$ and $\boldsymbol{b}_{0n+1}$ through the following transformation formulae:

$$\begin{aligned} \boldsymbol{\pi}^t_{n+1} &= -j\boldsymbol{F}^t_{n+1} \cdot \boldsymbol{\Pi}^t_{n+1} \cdot \boldsymbol{F}^t_{n+1} + j\Psi_{0n+1}\boldsymbol{F}^t_{n+1}, \\ \boldsymbol{B}_{tn+1} &= -j\boldsymbol{F}^t_{n+1} \cdot \boldsymbol{b}_{0n+1} + jS_0\nabla_X\theta_{n+1} - j\partial_{\boldsymbol{\Phi}}\Psi_{0n+1}. \end{aligned} \tag{52}$$

Remark 5.3 (*Adiabatic thermo-hyperelasticity*). Recall, that in general, the computational analysis of adiabatic problems within the spatial setting does not require a $\mathscr{C}^0$-continuous interpolation of the temperature field. Since the heat flux $\boldsymbol{Q}$ and with it a possible explicit dependence on the temperature gradient vanish in the adiabatic case, there is no obvious need to introduce the temperature as a nodal degree of freedom. For the material motion problem, however, the calculation of the material volume forces $\boldsymbol{B}_{tn+1}$

according to Eq. (52) essentially relies on the temperature gradient $\nabla_X \theta_{n+1}$, irrespective of the incorporation of a heat flux. The above-suggested $\mathscr{C}^0$-continuous interpolation of the temperature field is thus mandatory in the context of the material force method.

6. Examples

Finally, we turn to the elaboration of the derived thermo-hyperelastic finite element formulation by means of a number of selected examples. To this end, we introduce the following free energy function for thermo-hyperelastic materials,

$$\begin{aligned} \Psi_0 = & \frac{\lambda}{2} \ln^2 J + \frac{\mu}{2} [\boldsymbol{b} - \boldsymbol{I}] : \boldsymbol{I} - \mu \ln J && \text{mechanical part,} \\ & - 3\alpha\kappa [\theta - \theta_0] \frac{\ln J}{J} && \text{thermo-mechanical coupling,} \\ & + c_0 \left[\theta - \theta_0 - \theta \ln \frac{\theta}{\theta_0} \right] - [\theta - \theta_0] S^\circ && \text{thermal part,} \end{aligned} \tag{53}$$

whereby the first three terms represent the classical free energy function of Neo–Hooke type characterized through the two Lamé constants λ and μ. The fourth term introduces a thermo-mechanical coupling in terms of the thermal expansion coefficient α weighting the product of the bulk modulus κ and the difference between the current temperature θ and the reference temperature θ_0. The fifth term finally accounts for the purely thermal behavior in terms of the specific heat capacity c_0 and the last term define the absolute entropy density S° at the reference temperature θ_0. According to the general constitutive equation (9), the first Piola–Kirchhoff stress can be derived as thermodynamically conjugate variable to the spatial motion deformation gradient as $\boldsymbol{\Pi}^t = D_{\boldsymbol{F}} \Psi_0$ and thus

$$\boldsymbol{\Pi}^t = [\lambda \ln J - \mu] \boldsymbol{F}^{-t} + \mu \boldsymbol{F} - \frac{3\alpha\kappa}{J} [\theta - \theta_0][1 - \ln J] \boldsymbol{F}^{-t}. \tag{54}$$

Moreover, we assume the material heat flux $\boldsymbol{Q}$ to obey Fourier's law

$$\boldsymbol{Q} = -K_0 \boldsymbol{G} \cdot \nabla_X \theta \tag{55}$$

introducing a materially isotropic behavior in terms of the conductivity K_0, the material metric $\boldsymbol{G}$ and the material temperature gradient $\nabla_X \theta$. The convective part of the dissipation inequality $\mathsf{D}_0^{\text{con}} = -\boldsymbol{Q} \cdot \nabla_X \ln \theta \geqslant 0$ is thus a priori satisfied for the materially isotropic conductivity being strictly nonnegative as $K_0 \geqslant 0$. With the above definitions at hand, the derivatives of the momentum flux $\boldsymbol{\Pi}^t$, the resulting thermo-mechanical coupling term $\mathscr{Q}_0^{\text{mech}}$ and the heat flux $\boldsymbol{Q}$ with respect to the deformation gradient $\boldsymbol{F}$, the temperature θ and the temperature gradient $\nabla_X \theta$ which are essentially needed to compute the global tangential stiffness matrix according to Eq. (A.3) can be expressed as follows:

$$\begin{aligned} D_{\boldsymbol{F}} \boldsymbol{\Pi}^t &= \mu \boldsymbol{I} \overline{\otimes} \boldsymbol{I} + \lambda \boldsymbol{F}^{-t} \otimes \boldsymbol{F}^{-t} - [\lambda \ln J - \mu] \boldsymbol{F}^{-t} \underline{\otimes} \boldsymbol{F}^{-1}, \\ D_0 \boldsymbol{\Pi}^t &= -\frac{3\alpha\kappa}{J} [1 - \ln J] \boldsymbol{F}^{-t}, \\ D_{\boldsymbol{F}} \mathscr{Q}_0^{\text{mech}} &= \theta \frac{3\alpha\kappa}{J^2} [[3 - 2\ln J] \operatorname{div} \boldsymbol{v} - [1 - \ln J] D_J (D_t J)] J \boldsymbol{F}^{-t}, \\ D_0 \mathscr{Q}_0^{\text{mech}} &= -\frac{3\alpha\kappa}{J} [1 - \ln J] \operatorname{div} \boldsymbol{v}, \\ D_{\nabla_{X^0}} \boldsymbol{Q} &= -K_0 \boldsymbol{G}. \end{aligned} \tag{56}$$

The $D_{\boldsymbol{F}}\boldsymbol{\Pi}^t$ term of Eq. $(56)_1$ is typically introduced as sum of the geometric and the material part of the classical tangential stiffness matrix, whereby the component representation of the nonstandard dyadic products $\overline{\otimes}$ and $\underline{\otimes}$ reads $\{\bullet\,\overline{\otimes}\,\circ\}_{ijkl} = \{\bullet\}_{ik} \otimes \{\circ\}_{jl}$ and $\{\bullet\,\underline{\otimes}\,\circ\}_{ijkl} = \{\bullet\}_{il} \otimes \{\circ\}_{jk}$. Moreover, we have made use of the following transformation formula $\boldsymbol{F}^{-t} : D_t\boldsymbol{F} = \operatorname{div}\boldsymbol{v}$ in Eqs. $(56)_3$ and $(56)_4$. Recall that with the temporal discretization based on the traditional Euler backward method as suggested in Section 5, the temperature dependent term $D_J(D_tJ)$ of Eq. $(56)_3$ typically simplifies to $D_J(D_tJ) = 1/\Delta t$.

Remark 6.1 (*Isotropic heat flow*). Observe that in the present contribution, we assume the heat flux to be isotropic in the reference configuration as $\boldsymbol{Q} = -K_0\boldsymbol{G}\cdot\nabla_X\theta$ or alternatively $\boldsymbol{q} = -jK_0\boldsymbol{b}\cdot\nabla_x\theta$. In the related literature, however, we typically find a spatially isotropic rather than a materially isotropic behavior as $\boldsymbol{q} = -k_t\boldsymbol{g}\cdot\nabla_x\theta$ which corresponds to an anisotropic behavior in the reference configuration in the context of finite thermo-elasticity as $\boldsymbol{Q} = -Jk_t\boldsymbol{C}^{-1}\cdot\nabla_X\theta$, see e.g. Miehe [23,24], Reese and Wriggers [30] or Simo [33].

Remark 6.2 (*Absolute entropy*). We have to introduce an absolute entropy density S° in the free energy function Ψ_0. Otherwise the definition of the entropy density $S_0 = -D_0\Psi_0$ would only represents the change of the entropy in the system and this would lead to internal material forces $\boldsymbol{B}_t^{\text{int}}$ which depends on the reference temperature θ_0. Because we restrict our analysis in this section to materials with constant specific heat capacity c_0 the change of the temperature has to be moderate. Otherwise we have to address the temperature dependency of the heat capacity.

6.1. Bi-material bar

As a first example we consider a bi-material bar under tension with plane strain constraint. The material parameters of the left half of the bar correspond roughly to steel and are given in the following table,

Young's modulus E	205 000	$\left[\frac{\text{N}}{\text{mm}^2}\right]$
Poisson's ratio ν	0.29	
Density ρ_0	7.85×10^{-3}	$\left[\frac{\text{g}}{\text{mm}^3}\right]$
Thermal expansion coefficient α	11.5×10^{-6}	$\left[\frac{1}{K}\right]$
Thermal conductivity K_0	0.0498	$\left[\frac{\text{N}}{\text{ms K}}\right]$
Heat capacity c_0	3.8151	$\left[\frac{\text{N}}{\text{mm}^2\,\text{K}}\right]$
Reference temperature θ_0	298	[K]
Absolute entropy S°_{Fe}	3.8374	$\left[\frac{\text{N}}{\text{mm}^2\,\text{K}}\right]$

whereas the material parameters of the right half correspond roughly to an aluminium alloy, which are given below.

Young's modulus E Poisson's ratio ν	72 000 0.33	$\left[\frac{\mathrm{N}}{\mathrm{mm}^2}\right]$
Density ρ_0	2.81×10^{-3}	$\left[\frac{\mathrm{g}}{\mathrm{mm}^3}\right]$
Thermal expansion coefficient α	23.6×10^{-6}	$\left[\frac{1}{K}\right]$
Thermal conductivity K_0	0.130	$\left[\frac{\mathrm{N}}{\mathrm{ms\,K}}\right]$
Heat capacity c_0	2.6976	$\left[\frac{\mathrm{N}}{\mathrm{mm}^2\,\mathrm{K}}\right]$
Reference temperature θ_0	298	[K]
Absolute entropy S°_{Al}	2.9473	$\left[\frac{\mathrm{N}}{\mathrm{mm}^2\,\mathrm{K}}\right]$

The specimen is discretized by bi-linear Q1-elements. A constant elongation is applied at the left and right end of the bar within a very short first time step $\Delta t = 0.01$ and afterwards the elongation is kept constant. Due to the volatile change of the material parameters at the interface an inhomogeneous temperature field is induced by the external mechanical load. This results in a heat flux which equalizes the temperature differences within the bar over the time.

To point out the evolution of the material volume forces $\boldsymbol{B}_t$ we split the discrete material node point (surface) forces $\mathbf{F}^h_{\mathrm{sur}}$, given by Eq. (51), into an internal part

$$\mathbf{F}^{\varphi h}_{\mathrm{int}I} = \mathop{\mathbf{A}}_{e=1}^{n_{\mathrm{el}}} \int_{\mathscr{B}^e_t} \nabla_x N^i_{\Phi} \cdot \boldsymbol{\pi}_{n+1}\, \mathrm{d}v, \tag{57}$$

and a volume part

$$\mathbf{F}^{\varphi h}_{\mathrm{vol}I} = \mathop{\mathbf{A}}_{e=1}^{n_{\mathrm{el}}} \int_{\mathscr{B}^e_t} N^i_{\Phi} \boldsymbol{B}_{tn+1}\, \mathrm{d}v. \tag{58}$$

The computed discrete material node point (surface) forces 'SUR', the internal part 'INT' and the volume part 'VOL' in the vicinity of the interface are depicted in Fig. 3 for three different times $t = 0.01$, 1, 100. Thereby, we have applied a different scaling of the individual contributions 'SUR', 'INT' and 'VOL' for the sake of visualization. The distributions of the relative temperature $\Delta\theta$ are given as contour plots in Fig. 3.

After the mechanical load is applied within the first time step ($t = 0.01$) relatively large temperature gradients $\nabla_X \theta_{n+1}$ are observed in the vicinity of the interface which causes material node point volume forces 'VOL'. These vanish as time evolves due to the heat flux so that the resulting discrete material node point (surface) forces 'SUR' are dominated by their internal part 'INT'. Nevertheless, for this particular example, the contribution of the discrete material volume forces 'VOL' is always small compared to the internal forces 'INT' which are caused by the prescribed material inhomogeneity.

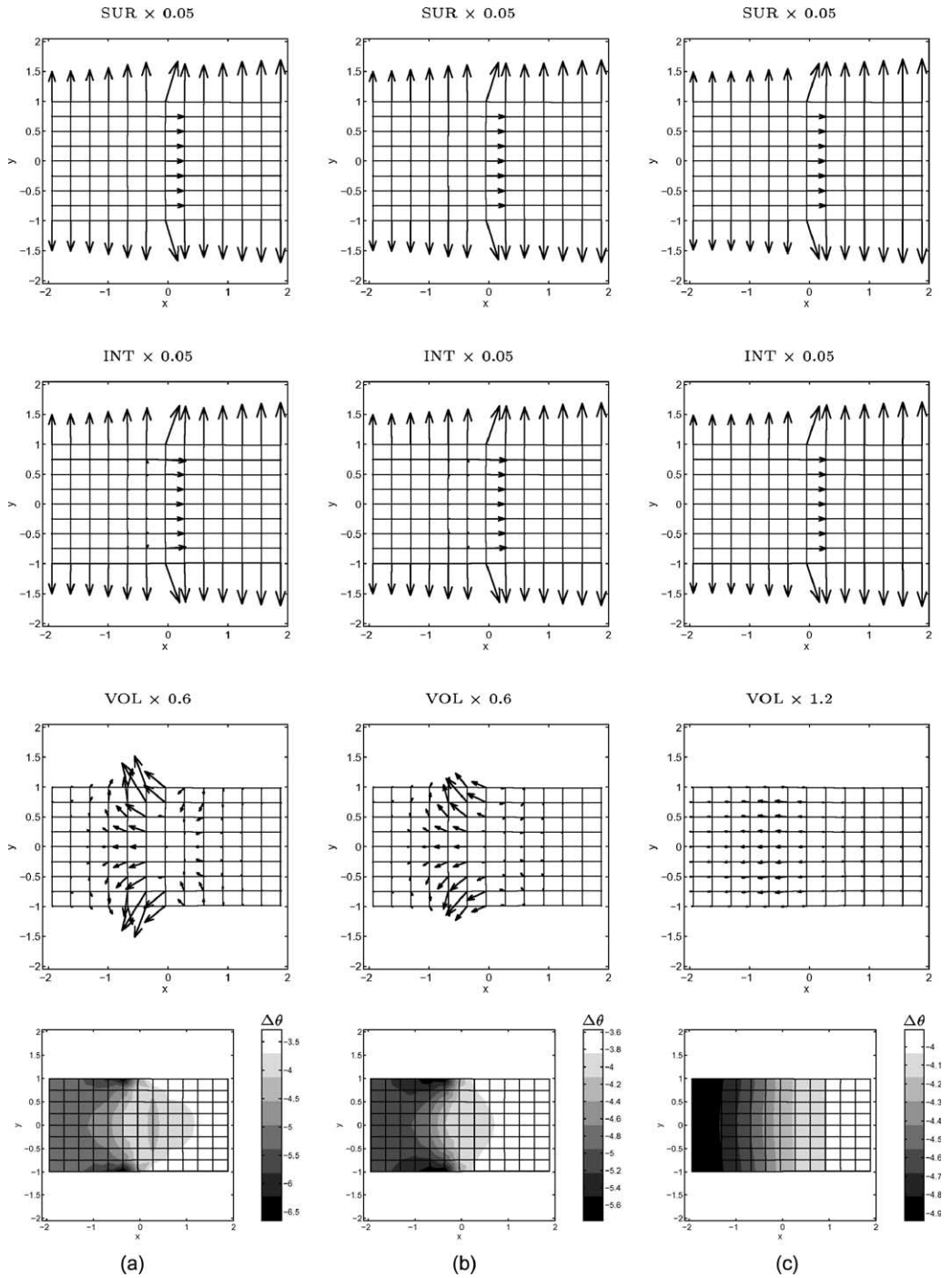

Fig. 3. Discrete material node point surface, internal and volume forces and temperature distribution in the vicinity of the interface at times $t =$ (a) 0.01, (b) 1, (c) 100.

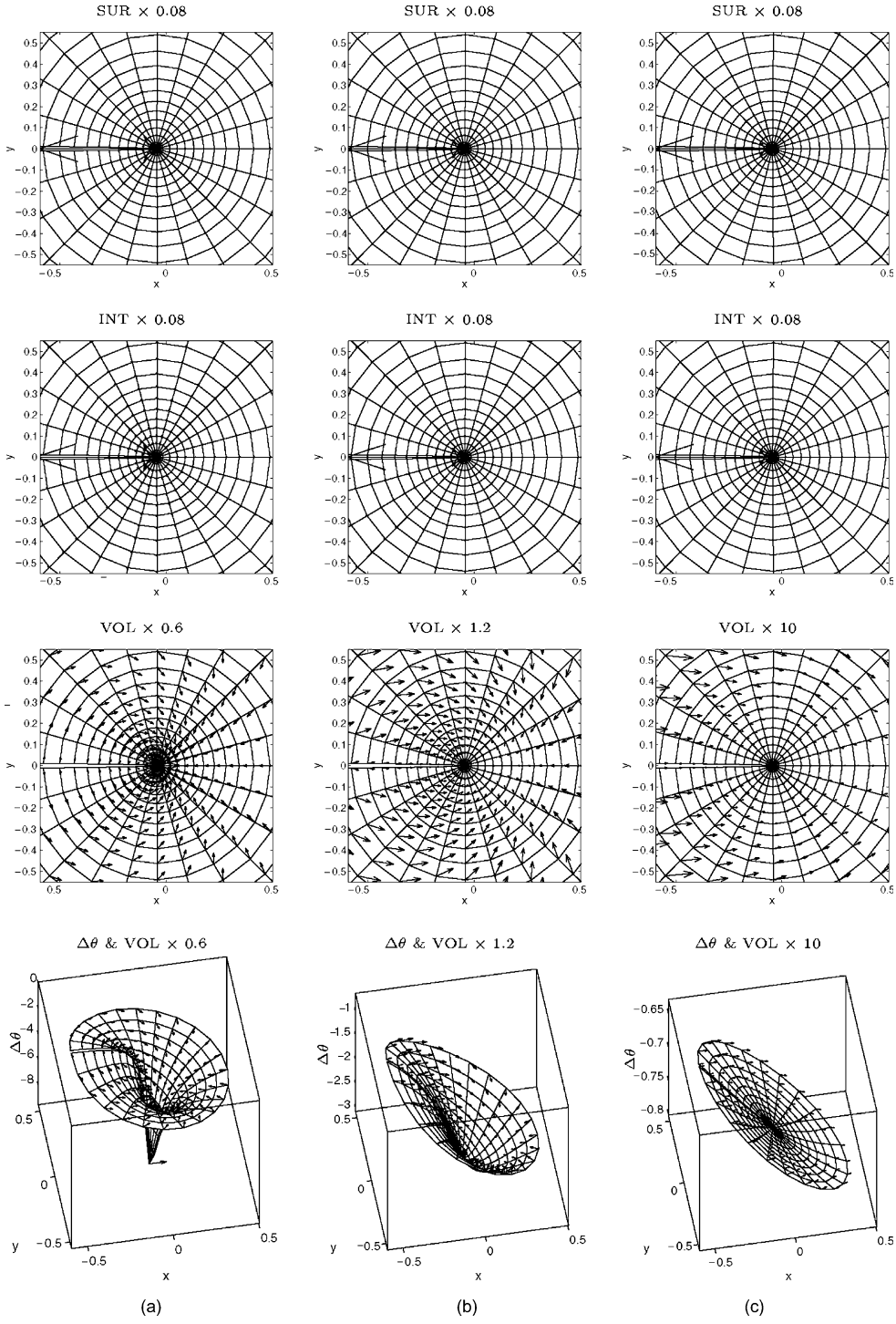

Fig. 4. Discrete material node point surface, internal and volume forces and temperature distribution in the vicinity of the crack tip at times $t =$ (a) 0.01, (b) 1, (c) 100.

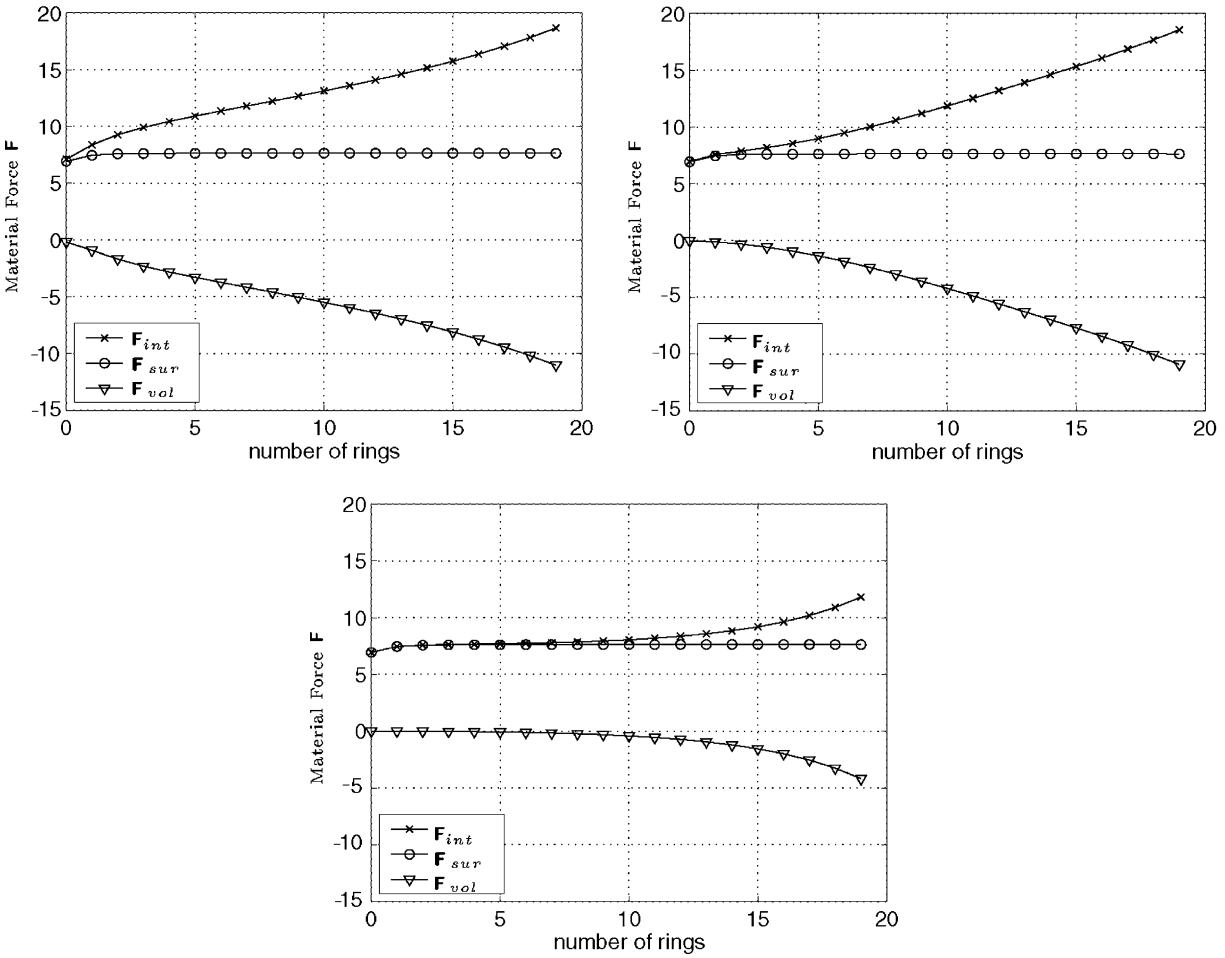

Fig. 5. Material forces at different time states $t = 0.01$, 1, 100.

6.2. Specimen with crack

As a second example we want to discuss a single edge notched tension specimen typically used in fracture mechanics. The height to width ratio is set to $H/W = 3$ and the ratio of crack length to width is $a/W = 0.5$. The specimen is discretized by bilinear Q1-elements and the mesh is heavily refined around the crack tip. The elements which are connected to the crack tip are P1-elements. The material is modeled with the parameters given in the previous section which roughly correspond to an aluminium alloy. A constant symmetric elongation of totally 0.1667% of the height W is applied at the top and bottom of the specimen within the first very short time step $\Delta t = 0.01$. The computed discrete material node point/surface forces 'SUR', the internal part 'INT', the volume part 'VOL' and the temperature distribution $\Delta\Theta$ in the vicinity of the crack tip are shown in Fig. 4 at three different time states $t = 0.01$, 1, 100.

Similar to the interface problem we observe steep temperature gradients $\nabla_X \theta$ after the load is applied within the first time step ($t = 0.01$). This results in large material node point volume forces 'VOL', which decreases over the time due to the heat flux with the specimen.

We now apply our improvement of the material force method for the vectorial J-Integral evaluation, as proposed in [6], which essentially consists of the summation of the material forces over a given subdomain V_0 enclosing the crack tip, except those which are associated with the regular, i.e. nonsingular, part of the boundary ∂V_0^r. This reads

$$-\boldsymbol{J} = \mathbf{F}_{\text{sur}} = \sum_{i=1}^{\overline{n}_{\text{np}}} \mathop{\mathbf{A}}_{e=1}^{n_{\text{el}}} \int_{\mathscr{B}_t^e} \nabla_x N_{\Phi}^i \cdot \boldsymbol{\pi}_{n+1} - N_{\Phi}^i \boldsymbol{B}_{tn+1} \, \mathrm{d}v, \tag{59}$$

where $\overline{n}_{\text{np}}$ is the number of all nodes lying in the subdomain $V_0 \setminus \partial V_0^r$.

We also introduce the split of the discrete material node point (surface) force $\mathbf{F}_{\text{sur}}$ into an internal part $\mathbf{F}_{\text{int}}$ and a volume part $\mathbf{F}_{\text{vol}}$ in this case analogous to Eqs. (57) and (58). As given subdomains for Eq. (59) we simply use those subdomains defined by different numbers of element rings in the vicinity of the crack tip. The resulting material forces for three different times $t = 0.01$, 1, 100 are shown in Fig. 5.

Although the internal part $\mathbf{F}_{\text{int}}$ and the volume part $\mathbf{F}_{\text{vol}}$ of the material surface force are domain dependent due to the temperature gradient $\nabla_X \theta$ the resulting material surface force $\mathbf{F}_{\text{sur}}$ behaves domain independent.

7. Conclusion

The objective of this work was the numerical analysis of material forces of thermo-hyperelasticity constitutes where thermal effects can be understood as a source of inhomogeneity. This leads to distributed volume forces $\boldsymbol{B}_t^{\text{int}}$ which are generally different from zero in the material setting. This effect is demonstrated by a bi-material bar under tension load and a specimen with a crack under Mode I loading. The evaluation of the single material surface force acting at the crack tip is domain independent and therefore numerically very attractive.

In the purely thermo-hyperelastic case considered herein, thermomechanical coupling in the form of the Gough–Joule effect leads to a decrease of the temperature in the vicinity of the crack tip. A more realistic physical model, which is currently being developed in our research group, should, of course, include effects of inelasticity. An inelastic material behaviour would then lead to a so-called 'hot spot' due to the pronounced effect of dissipation at the crack tip.

Appendix A

The discrete coupled nonlinear system of equations of the spatial motion problem is solved in a monolithic sense with the help of an incremental iterative Newton–Raphson solution strategy. The discrete balance of momentum $(41)_1$ and the discrete balance of energy $(41)_2$ are thus solved simultaneously at time t_{n+1}. Consequently, the $k+1$th iterate of the Newton iteration can be expressed as

$$\begin{aligned} \mathbf{r}_{In+1}^{\varphi k+1} &= \mathbf{r}_{In+1}^{\varphi k} + \mathrm{d}\mathbf{r}_I^{\varphi} \doteq \mathbf{0} \quad \forall I = 1, n_{\text{np}}, \\ \mathrm{r}_{Jn+1}^{\vartheta k+1} &= \mathrm{r}_{Jn+1}^{\vartheta k} + \mathrm{d}\mathrm{r}_J^{\vartheta} \doteq 0 \quad \forall J = 1, n_{\text{np}}, \end{aligned} \tag{A.1}$$

whereby $\mathrm{d}\mathbf{r}_I^{\varphi}$ and $\mathrm{d}\mathrm{r}_J^{\vartheta}$ denote the iterative residue which are based on the consistent linearization of the governing equations.

$$\begin{aligned} \mathrm{d}\mathbf{r}_I^{\varphi} &= \sum_{K=1}^{n_{\mathrm{np}}} \mathbf{K}_{IK}^{\varphi\varphi} \cdot \mathrm{d}\boldsymbol{\varphi}_K + \sum_{L=1}^{n_{\mathrm{np}}} \mathbf{K}_{IL}^{\varphi 0} \mathrm{d}\theta_L \quad \forall I = 1, n_{\mathrm{np}}, \\ \mathrm{d}\mathrm{r}_J^{\theta} &= \sum_{K=1}^{n_{\mathrm{np}}} \mathbf{K}_{JK}^{0\varphi} \cdot \mathrm{d}\boldsymbol{\varphi}_K + \sum_{L=1}^{n_{\mathrm{np}}} K_{JL}^{00} \mathrm{d}\theta_L \quad \forall J = 1, n_{\mathrm{np}}. \end{aligned} \tag{A.2}$$

They can be expressed in terms of the iteration matrices $\mathbf{K}_{IK}^{\varphi\varphi}$, $\mathbf{K}_{IL}^{\varphi 0}$, $\mathbf{K}_{JK}^{0\varphi}$, K_{JL}^{00}, and the incremental changes of the global vector of unknowns $\mathrm{d}\boldsymbol{\varphi}_K$ and $\mathrm{d}\theta_L$.

For the problem at hand, these iteration matrices which can be interpreted as submatrices of the global tangential stiffness matrix take the following format:

$$\begin{aligned} \mathbf{K}_{IK}^{\varphi\varphi} &= \frac{\partial \mathbf{r}_I^{\varphi}}{\partial \boldsymbol{\varphi}_K} = \mathop{\mathsf{A}}_{e=1}^{n_{\mathrm{el}}} \int_{\mathscr{B}_0} N^i \rho_0 \frac{1}{\Delta t^2} \boldsymbol{I} N^k + \nabla_X N^i \cdot D_{\boldsymbol{F}} \boldsymbol{\Pi}^t \cdot \nabla_X N^k \, \mathrm{d}V, \\ \mathbf{K}_{IL}^{\varphi 0} &= \frac{\partial \mathbf{r}_I^{\varphi}}{\partial \theta_L} = \mathop{\mathsf{A}}_{e=1}^{n_{\mathrm{el}}} \int_{\mathscr{B}_0} \nabla_X N^i \cdot D_0 \boldsymbol{\Pi}^t N^l \, \mathrm{d}V, \\ \mathbf{K}_{JK}^{0\varphi} &= \frac{\partial \mathrm{r}_J^{\theta}}{\partial \boldsymbol{\varphi}_K} = \mathop{\mathsf{A}}_{e=1}^{n_{\mathrm{el}}} \int_{\mathscr{B}_0} -N^j D_{\boldsymbol{F}} \mathscr{Q}_0^{\mathrm{mech}} \cdot \nabla_X N^k \, \mathrm{d}V, \\ \mathbf{K}_{JL}^{00} &= \frac{\partial \mathrm{r}_J^{\theta}}{\partial \theta_L} = \mathop{\mathsf{A}}_{e=1}^{n_{\mathrm{el}}} \int_{\mathscr{B}_0} N^j c_0 \frac{1}{\Delta t} N^l - N^j D_0 \mathscr{Q}_0^{\mathrm{mech}} N^l + \nabla_X N^j \cdot D_{\nabla_X 0} \boldsymbol{Q} \cdot \nabla_X N^l \, \mathrm{d}V. \end{aligned} \tag{A.3}$$

Therein, the first terms of Eqs. $(A.3)_1$ and $(A.3)_4$ illustrate the time-dependent nature of the problem. They represent the consistent mass and capacity matrix, respectively. The second term of $(A.3)_1$ corresponds to the classical structural stiffness. Eq. $(A.3)_2$ reflects the thermal influence in the constitutive equation. The indirect influence of the changes in temperature on the deformation field and on the temperature field introduced through the Gough–Joule effect is reflected through Eq. $(A.3)_3$ and the second term in $(A.3)_4$. The last term in Eq. $(A.3)_4$ accounts for heat convection. The above introduced derivatives of the momentum flux $\boldsymbol{\Pi}^t$, the thermo-mechanical coupling term $\mathscr{Q}_0^{\mathrm{mech}}$ and the heat flux $\boldsymbol{Q}$ with respect to the deformation gradient $\boldsymbol{F}$, the temperature θ and the temperature gradient $\nabla_X \theta$ depend on the choice of the individual constitutive equations. A particular examplification is given in Section 6. The solution of the linearized system of Eqs. (A.1) finally defines the iterative update for the increments of the global unknowns $\boldsymbol{\varphi}_I$ and θ_J.

$$\begin{aligned} \Delta\boldsymbol{\varphi}_I &= \Delta\boldsymbol{\varphi}_I + \mathrm{d}\boldsymbol{\varphi}_I \quad \forall I = 1, n_{\mathrm{np}}, \\ \Delta\theta_J &= \Delta\theta_J + \mathrm{d}\boldsymbol{\theta}_J \quad \forall J = 1, n_{\mathrm{np}}. \end{aligned} \tag{A.4}$$

Remark A.1 (*Transient terms in the linearized residual*). Recall, that when considering the balance of momentum in the quasi-static sense, the term $N^I \rho_0 / \Delta t^2 \boldsymbol{I} N^K$ of Eq. $(A.3)_1$ vanishes identically.

References

[1] F. Armero, J.C. Simo, A new unconditionally stable fractional step method for non-linear coupled thermo-mechanical problems, Int. J. Num. Methods Engrg. 35 (1992) 737–766.

[2] H. Askes, E. Kuhl, P. Steinmann, An ALE formulation based on spatial and material settings of continuum mechanics. Part 2: Classification and applications, Comput. Methods Appl. Mech. Engrg., in press.

[3] H. Askes, E. Kuhl, P. Steinmann, Arbitrary Lagrangian–Eulerian (ALE) mesh optimization by equilibration of discrete material forces, in: E. Oñate, D.R.J. Owen, (Eds.), Proceedings of COMPLAS VII, Barcelona, Spain, 7–10 April 2003, CIMNE, Barcelona, Spain, 2003.

[4] M. Braun, Configurational forces induced by finite-element discretization, Proc. Estonian Acad. Sci. Phys. Math. 46 (1997) 24–31.
[5] B.D. Coleman, W. Noll, The thermodynamics of elastic materials with heat conduction and viscosity, Arch. Rat. Mech. Anal. 13 (1963) 167–178.
[6] R. Denzer, F.J. Barth, P. Steinmann, Studies in elastic fracture mechanics based on the material force method, Int. J. Num. Methods Engrg. 58 (2003) 1817–1835.
[7] J.D. Eshelby, The force on an elastic singularity, Philos. Trans. Roy. Soc. London 244 (1951) 87–112.
[8] J.D. Eshelby, The determination of the elastic field of an ellipsoidal inclusion and related problems, Proc. Roy. Soc. London A 241 (1957) 376–396.
[9] Govindjee, S., Firestone tire analysis, Internal Report, Lafayette, CA, 2001.
[10] M.E. Gurtin, Configurational Forces as Basic Concepts of Continuum Physics, Springer Verlag, New York–Berlin–Heidelberg, 2000.
[11] P. Haupt, Continuum Mechanics and Theory of Materials, Springer Verlag, Berlin–Heidelberg–New York, 2000.
[12] A. Ibrahimbegovic, L. Chorfi, F. Gharzeddine, Thermomechanical coupling at finite elastic strain: covariant formulation and numerical implementation, Commun. Num. Methods Engrg. 17 (2001) 275–289.
[13] R. Kienzler, G. Herrmann, Mechanics in Material Space with Applications to Defect and Fracture Mechanics, Springer Verlag, Berlin–Heidelberg–New York, 2000.
[14] E. Kuhl, H. Askes, P. Steinmann, An ALE formulation based on spatial and material settings of continuum mechanics. Part 1: Generic hyperelastic formulation. Comput. Methods Appl. Mech. Engrg., in press.
[15] E. Kuhl, P. Steinmann, Material forces in open system mechanics. Comput. Methods Appl. Mech. Engrg., accepted for publication.
[16] E. Kuhl, P. Steinmann, On spatial and material settings of thermo-hyperelastodynamics for open systems, Acta Mech. 160 (2003) 179–217.
[17] T. Liebe, R. Denzer, P. Steinmann, Application of the material force method to isotropic continuum damage, Computat. Mech. 30 (2003) 171–184.
[18] I.S. Liu, Continuum Mechanics, Springer Verlag, Berlin–Heidelberg–New York, 2002.
[19] G.A. Maugin, Material Inhomogeneities in Elasticity, Chapman & Hall, London, 1993.
[20] G.A. Maugin, Material forces: Concepts and Applications, Appl. Mech. Rev. 48 (1995) 213–245.
[21] G.A. Maugin, The Thermomechanics of Nonlinear Irreversible Behaviors, World Scientific Publishing Co., 1999.
[22] C. Miehe, Zur numerischen Behandlung thermomechanischer Prozesse, Dissertation, Universität Hannover, Institut für Baumechanik und Numerische Mechanik, Bericht-Nr. 88/6, 1988.
[23] C. Miehe, Kanonische Modelle multiplikativer Elasto-Plastizität—Thermodynamische Formulierung und Numerische Implementation. Habilitationsschrift, Institut für Baumechanik und Numerische Mechanik, Universität Hannover, Bericht-Nr. 93/1, 1993.
[24] C. Miehe, Entropic thermoelasticity at finite strains. Aspects of the formulation and numerical implementation, Comput. Methods Appl. Mech. Engrg. 120 (1995) 243–269.
[25] R. Mueller, G.A. Maugin, On material forces and finite element discretizations, Comput. Mech. 29 (2002) 52–60.
[26] R. Müller, S. Kolling, D. Gross, On configurational forces in the context of the finite element method, Int. J. Num. Methods Engrg. 53 (2002) 1557–1574.
[27] J.T. Oden, Finite Elements of Nonlinear Continua, Advanced Engineering Series, McGraw-Hill, 1972.
[28] S. Reese, Thermomechanische Modellierung gummiartiger Polymerstrukturen, Habilitationsschrift, Institut für Baumechanik und Numerische Mechanik, Universität Hannover, Bericht-Nr. F01/4, 2001.
[29] S. Reese, S. Govindjee, Theoretical and numerical aspects in the thermo-viscoelastic material behavior of rubber-like polymers, Mech. Time-dependent Mater. 1 (1998) 357–396.
[30] S. Reese, P. Wriggers, Thermo-viscoelastic material behaviour at finite deformations with temperature-dependent material parameters, ZAMM 78 (1998) S157–S160.
[31] C.F. Shih, B. Moran, T. Nakamura, Energy release rate along a three-dimensional front in a thermally stressed body, Int. J. Fract. 30 (1986) 79–102.
[32] M. Silhavý, The Mechanics and Thermodynamics of Continuous Media, Springer Verlag, New York–Berlin–Heidelberg, 1997.
[33] J.C. Simo, Numerical analysis and simulation of plasticity, in: P.G. Ciarlet, J.L. Lions (Eds.), Handbook of Numerical Analysis, vol. VI, North-Holland, Elsevier, 1998, pp. 183–199.
[34] J.C. Simo, C. Miehe, Associative coupled thermo-plasticity at finite strains: Formulation, numerical analysis and implementation, Comput. Methods Appl. Mech. Engrg. 98 (1992) 41–104.
[35] P. Steinmann, Application of material forces to hyperelastostatic fracture mechanics. I. Continuum mechanical setting, Int. J. Solids Struct. 37 (2000) 7371–7391.
[36] P. Steinmann, On spatial and material settings of hyperelastodynamics, Acta Mech. 156 (2002) 193–218.
[37] P. Steinmann, On spatial and material settings of thermo-hyperelastodynamics, J. Elasticity 66 (2002) 109–157.

[38] P. Steinmann, D. Ackermann, F.J. Barth, Application of material forces to hyperelastostatic fracture mechanics. II. Computational setting, Int. J. Solids Struct. 38 (2001) 5509–5526.
[39] C. Truesdell, W. Noll, The non-linear field theories of mechanics, in: S. Flügge (Ed.), Handbuch der Physik, vol. III/3, Springer Verlag, Berlin, 1965.
[40] C. Truesdell, R. Toupin, The classical field theories, in: S. Flügge (Ed.), Handbuch der Physik, vol. III/1, Springer Verlag, Berlin, 1960.